Flow Turbulence Combust (2008) 81:337–367
DOI 10.1007/s10494-008-9134-6

One Equation Model for Turbulent Channel Flow with Second Order Viscoelastic Corrections

F. T. Pinho · B. Sadanandan · R. Sureshkumar

Received: 18 June 2007 / Accepted: 16 January 2008 / Published online: 5 March 2008

Abstract A modified second order viscoelastic constitutive equation is used to derive a k–l type turbulence closure to qualitatively assess the effects of elastic stresses on fully-developed channel flow. Specifically, the second order correction to the Newtonian constitutive equation gives rise to a new term in the momentum equation involving the time-averaged elastic shear stress and in the turbulent kinetic energy transport equation quantifying the interaction between the fluctuating elastic stress and rate of strain tensors, denoted by P_w, for which a closure is developed and tested. This closure is based on arguments of isotropic turbulence and equilibrium in boundary layer flows and a priori P_w could be either positive or negative. When P_w is positive, it acts to reduce the production of turbulent kinetic energy and the turbulence model predictions qualitatively agree with direct numerical simulation (DNS) results obtained for more realistic viscoelastic fluid models with memory which exhibit drag reduction. In contrast, $P_w<0$ leads to a drag increase and numerical breakdown of the model occurs at very low values of the Deborah number, which signifies the ratio of elastic to viscous stresses. Limitations of the turbulence model primarily stem from the inadequacy of the k–l formulation rather than from the closure for P_w. An alternative closure for P_w, mimicking the viscoelastic stress work predicted by DNS using the Finitely Extensible Nonlinear Elastic-Peterlin fluid model, which is mostly characterized by $P_w>0$ but has also a small region of negative P_w in the buffer layer, was also successfully tested. This second model for P_w leads to predictions of drag reduction, in spite of the enhancement of turbulence production very close to the wall, but the equilibrium conditions in the inertial sub-layer were not strictly maintained.

F. T. Pinho (✉)
CEFT, Faculdade de Engenharia, Universidade do Porto,
Rua Dr. Roberto Frias s/n, 4200-465 Porto, Portugal
e-mail: fpinho@fe.up.pt

F. T. Pinho
Universidade do Minho, Largo do Paço, 4704-553 Braga, Portugal

B. Sadanandan
Intel Corporation,
Hillsboro, OR 97124, USA

R. Sureshkumar
Department of Energy, Environmental and Chemical Engineering, Center for Materials Innovation,
Washington University, St. Louis, MO 63130, USA
e-mail: suresh@wustl.edu

Keywords Viscoelastic · Drag reduction · Second order constitutive equation · k–l model

Nomenclature

A	parameter of polymer work model, see (33)
b_{ij}	tensor defined in (28)
C_D	parameter of turbulence model, see (23)
C_k	parameter of k–l turbulence model
C_{ij}	time-average component of elastic stress tensor defined in (12)
D_k	Turbulent and molecular diffusion of turbulent kinetic energy, defined in (20b)
De	Deborah number based on bulk velocity of the flow
De_l	Deborah number of turbulence, $De_l = u\lambda/l$
De_τ	friction Deborah number, $De_\tau = u_\tau\lambda/H$
H	channel half-height
k	turbulent kinetic energy
l	length scale in turbulence in order of magnitude analysis and Prandtl's mixing length in turbulence model
p	pressure
P_k	Production of turbulent kinetic energy, defined in (20a)
P_w	Polymeric work, defined in (20d)
t	time
T_{ij}	designates a time-average tensor
u	scale of velocity fluctuations in order of magnitude analysis and streamwise velocity component in turbulence model equations
u_i	fluctuating velocity vector
$\hat{u}_i$	instantaneous velocity vector
u^*	streamwise velocity normalized by the friction velocity, $u^+ = u/u_\tau$
U_i	time-average velocity vector
u_τ	friction velocity in fully-developed channel flow
$\overline{uv}$	Reynolds shear stress
Re	Reynolds number based on bulk velocity of the flow
Re_l	Reynolds number of turbulence, $Re_l = ul/\upsilon_T$
Re_τ	friction Reynolds number, $Re_\tau = u_\tau H/\upsilon_T$
x	streamwise coordinate
x_i	general coordinate
v	wall-normal velocity component
w	spanwise velocity component
y	wall-normal coordinate
y^*	wall-normal coordinate normalized by physical coordinates, $y^* = y/H$
y^+	wall-normal coordinate normalized by wall coordinates, $y^+ = yu_\tau/\upsilon_T$
z	spanwise coordinate

Greek characters

β	ratio of solvent to total viscosities, $\beta = \upsilon_s/(\upsilon_s + \upsilon_p)$
δ_{ij}	Kronecker delta
ε	viscous dissipation of turbulent kinetic energy
ε_{ij}	rate of viscous dissipation of the Reynolds stress tensor $\overline{u_i u_j}$
ε_w	rate of viscous dissipation of turbulent kinetic energy at the wall, defined in (24)
$\dot{\gamma}_{ij}$	fluctuating rate of deformation tensor

$\hat{\dot{\gamma}}_{ij}$	instantaneous rate of deformation tensor
Γ_{ij}	time average rate of deformation tensor
η_p	viscosity coefficient of polymer
η_s	viscosity coefficient of Newtonian solvent
κ	von Kármán constant
λ	relaxation time of the fluid
λ_f	Taylor longitudinal microscale of turbulence
μ	ratio between production of turbulent kinetic energy and polymeric work
ρ	fluid density
σ_k	Turbulent Prandlt number associated with turbulent diffusion of k by the pressure and velocity fluctuations, see (21)
σ_{kp}	second turbulent Prandtl number associated with turbulent diffusion of k by the fluctuating elastic stresses, see (22)
$\tau_{ik,t}$	fluctuating total extra stress tensor
$\hat{\tau}_{ik,t}$	instantaneous total extra stress tensor
τ^e_{ij}	elastic part of the polymer tensor contribution to the total extra stress tensor
$\tau_{ik,p}$	fluctuating polymer tensor contribution to the total extra stress tensor
$\hat{\tau}_{ik,p}$	instantaneous polymer tensor contribution to the total extra stress tensor
$\upsilon_p = \eta_p / \rho$	kinematic viscosity of the polymer
$\upsilon_s = \eta_s / \rho$	kinematic viscosity of the Newtonian solvent
υ_T	total kinematic viscosity, $\upsilon_T = \upsilon_s + \upsilon_p$
Ψ_1	first normal stress difference coefficient
Ψ_2	second normal stress difference coefficient

1 Introduction

Over the last 10 years there has been a renewed effort towards understanding turbulent drag reduction (DR) in fully-developed pipe and channel flows of viscoelastic dilute polymer solutions. This has been accomplished in two ways: experimentally, using advanced optical diagnostic techniques such as laser-Doppler anemometry and particle image velocimetry [1–5], with the emphasis placed on investigating near-wall phenomena; numerically using direct numerical simulations (DNS) with a variety of rheological constitutive equations, such as the Oldroyd-B, Giesekus or the FENE-P models [5–10], amongst others to probe the coupling between turbulence and polymer conformation (or elastic stress) leading to DR.

These works provide a clear picture of the phenomenon of drag reduction and its relation with the fluid rheology and events, e.g. coherent structure dynamics, taking place in the various regions of the flow [11]. However, from a practical point of view the prediction of the behavior of specific viscoelastic fluids in different turbulent flows remains a challenge, because of the lack of robust turbulent closures to solve the time-averaged momentum and constitutive equations. DNS results have been only recently analyzed with a view to develop closures, such as the zero order model of Li et al. [12] and the first order model of Shaqfeh et al. [13], and there is still a lack of coupling between the DNS and the corresponding closures under development on one side, and the rheology of real drag-reducing fluids on the other.

The difficulties inherent to the development of single point closures for viscoelastic fluids based on differential viscoelastic constitutive equations, even with the help of DNS data, have inspired a more practical approach in which fluid properties that are considered relevant to DR are identified and they lead to the formulation of simple constitutive

equations which are subsequently used to develop single-point closures. This approach was used by Pinho and co-workers [14–16], who formulated several low Reynolds number k–ε type models and a Reynolds stress model on the basis of a modified Generalized Newtonian constitutive model that accounted for shear-thinning in shear viscosity and shear-thickening of the Trouton ratio. These turbulence models have shown to perform satisfactorily in fully-developed pipe and channel flows of polymer solutions and behave qualitatively well in homogeneous isotropic turbulence due to the modification of the molecular viscosity. Their constitutive equation is purely viscous and the capability of the turbulence models to accurately predict drag reduction in shear flow is essentially due to a new damping function. This damping function accounts for wall effects in various terms: within the context of a k–ε closure it corrects the average molecular viscosity and especially the eddy viscosity, whereas for the second order turbulence model it corrects the rate of dissipation of the Reynolds stress tensor (ε_{ij}) and the pressure strain. An innovative feature of the turbulence model and its damping function is that they depend on the rheology via its four parameters: the consistency and power indices of the shear viscosity and the consistency and power indices of the Trouton ratio. However, neither the transport equations nor the turbulence models contain any normal stress or memory effects associated with the viscoelasticity of the fluid.

In this work, starting from a relatively simple viscoelastic rheological constitutive equation, namely a simplified version of the "second order" fluid model that contains a second order correction to the Newtonian law, we derive a simple turbulence closure for boundary layer flows, based on Prandtl's one-equation k–l model for Newtonian fluids. Our objective is to investigate qualitatively the effects of elastic stresses on turbulent flow characteristics, and, in particular, to inquire whether they can help predict drag reduction and, if so, how significant the predicted DR effect would be. While such a model cannot be expected to quantitatively predict the flow behaviour of viscoelastic fluids in turbulent flows, it could be a useful tool to assess qualitatively the effect of viscoelasticity on the spatial correlations of velocity and stress fluctuations. Such information could help future developments of turbulent closures based on differential constitutive equations, such as the FENE-P model. As far as we are aware investigations on turbulence of second order fluids are scarce, one of the first carried out by Elata and Poreh [17]. In this early work the drag reduction was related to the appearance of an additional contribution to the extra shear stress, proportional to the vorticity correlation tensor and involving the two cross-viscosity coefficients, but opposite in sign to the molecular (viscous) and Reynolds stresses. Recently, in an attempt to understand the turbulent transition mechanisms for polymer solutions, Roy et al. [18] have used second to fourth order fluids to investigate the effect of polymers on the energy feedback from the unstable streaks to the streamwise counter-rotating vortices. They concluded that the reduction in critical Reynolds number observed for weakly elastic fluids can be predicted by second order fluids, whereas the subsequent increase for more elastic fluids requires models of at least third order. Both changes were found to be intimately connected with the response of the fluid to biaxial extensional deformation. In this work, we focus on incorporating second order (SO) corrections into a one equation model for turbulent channel flow to explore the influence of closure approximations employed for the terms arising from viscoelastic corrections on predicted DR. Of particular interest are the effects of the sign and magnitude of the correlation coefficient associated with the viscoelastic stress-velocity gradient correlation on the DR behavior. Since such correlations also arise when more sophisticated viscoelastic constitutive models are used, the insights obtained with the SO model could be useful as a limiting case scenario for relatively small DR values. From an engineering point of view,

the stress-velocity gradient correlation coefficient may be parameterized against experimental data for rheological and flow properties to obtain semi-empirical models for predicting the DR behavior.

The remaining of this paper is organized as follows: in Section 2 the governing equations and turbulence model are presented with new closures explained in detail. The model is tested in fully-developed channel flow in Section 3 and the main conclusions are drawn at the end.

2 Governing Equations and Turbulence Model

2.1 Fluid constitutive equation and momentum equation

In what follows instantaneous quantities are denoted by a hat, capital letters or an overbar designate time-average quantities and small letters or primes denote fluctuating quantities.

The turbulent flow is governed by the continuity and the momentum equations (1) and (2), respectively, which are here written in index notation.

$$\frac{\partial \hat{u}_i}{\partial x_i} = 0 \tag{1}$$

$$\rho\left[\frac{\partial \hat{u}_i}{\partial t} + \hat{u}_k \frac{\partial \hat{u}_i}{\partial x_k}\right] = -\frac{\partial \hat{p}}{\partial x_i} + \frac{\partial \hat{\tau}_{ik,t}}{\partial x_k} \tag{2}$$

As shown in (3) below, the total extra stress $\hat{\tau}_{ik,t}$ of the fluid in (2) is split into a Newtonian solvent component of viscosity coefficient η_s and a polymer additive stress component $\hat{\tau}_{ik,p}$, which in turn is modeled by (4). This could be the case for a solution of polymer molecules in a Newtonian solvent. In fact, (3) and (4) consist of the Newtonian model with a second-order correction related to the first normal stress difference coefficient (Ψ_1) [19]. This is not the classical second order fluid model since the term proportional to the square of the rate of deformation tensor $\left(\dot{\gamma}_{ij}\right)$ is not considered. Instead, although this version of the second order fluid has $\Psi_1 = 2\lambda\eta_p$ the second normal stress difference coefficient (Ψ_2) is null. This is not a severe simplification since for real fluids $|\Psi_2| << |\Psi_1|$ [20], but allows us to isolate first normal stress effects to better study their impact on turbulence. The fluctuating rate of deformation tensor is defined as $\dot{\gamma}_{ij} = \partial u_i/\partial x_j + \partial u_j/\partial x_i$, and the corresponding time-average quantity is denoted $\dot{\Gamma}_{ij}$. Time-averaged stresses are represented by T_{ij}.

Non-Newtonian behavior is characterized by several different phenomena, which can be of purely viscous nature as well as of elastic nature. The typical purely viscous non-Newtonian characteristic is a variable viscosity depending on the local rate of deformation, usually imparting a shear-thinning viscosity behavior, which is very common with polymer solutions and melts. Elasticity manifests itself in various ways: a memory effect, where the fluid responds with a time lag to an instantaneous forcing, strain-hardening in extensional deformations; but there are also deviations from the Newtonian behavior, such as the appearance of normal stresses in steady shear flow that are associated with elasticity and can also be explained by rheological constitutive equations devoid of memory effects, such as the retarded-motion expansions [20]. The second order fluid belongs to this category. With some well identified exceptions, retarded motion expansions are not so useful for engineering purposes given their limitations and limited rheology capabilities [20], but

provide valuable insight into problems. In this particular case it allows us to investigate the role of the first normal stress difference in turbulent flow, without the accompanying effect of memory that results from the use of more realistic viscoelastic differential constitutive equations, such as the Oldroyd-B, the FENE-P or Giesekus models, each of which has its own limitations and where memory and elastic stress effects are combined.

The second order fluid model is described by:

$$\hat{\tau}_{ij,t} = \eta_s \hat{\dot{\gamma}}_{ij} + \hat{\tau}_{ij,p} \tag{3}$$

$$\hat{\tau}_{ij,p} = \eta_p \hat{\dot{\gamma}}_{ij} - \eta_p \lambda \hat{\dot{\gamma}}_{ij(1)} \tag{4}$$

Equation (4) explicitly breaks the polymer stress into a viscous component $= \eta_p \hat{\dot{\gamma}}_{ij}$ having a polymer viscosity coefficient η_p and the second order correction is an elastic contribution $\left(\hat{\tau}^e_{ij}\right)$ given by

$$\hat{\tau}^e_{ij} = \eta_p \lambda \hat{\dot{\gamma}}_{ij_{(1)}} \tag{5}$$

where λ is a parameter of the constitutive equation having dimensions of time and $\hat{\dot{\gamma}}_{ij_{(1)}}$ is the upper convected derivative of the deformation rate tensor $\hat{\dot{\gamma}}_{ij}$ given by (6).

$$\hat{\dot{\gamma}}_{ij_{(1)}} = \frac{\partial \hat{\dot{\gamma}}_{ij}}{\partial t} + \hat{u}_k \frac{\partial \hat{\dot{\gamma}}_{ij}}{\partial x_k} - \hat{\dot{\gamma}}_{jk} \frac{\partial \hat{u}_i}{\partial x_k} - \hat{\dot{\gamma}}_{ik} \frac{\partial \hat{u}_j}{\partial x_k} \tag{6}$$

Parameter λ is the ratio of the first normal stress difference coefficient in simple (homogeneous) shear flow to the viscosity coefficient. Since it has dimensions of time it is called a relaxation time for memory fluids, but in the context of models devoid of memory, such as the retarded motion expansion (the second order fluid belongs to this wider class of constitutive equations) such nomenclature is not so appropriate. In laminar flow this model parameter gives rise to a specific non-dimensional number, the Deborah number, the ratio of the magnitudes of the elastic to the viscous forces, a measure of the importance of the nonlinear terms on the flow, as will be seen at the end of Section 2.4.

After back-substitution the instantaneous momentum equation becomes:

$$\rho\left(\frac{\partial \hat{u}_i}{\partial t} + \hat{u}_j \frac{\partial \hat{u}_i}{\partial x_j}\right) = \frac{\partial}{\partial x_j}\left(-\hat{p}\delta_{ij} + \eta_s \hat{\dot{\gamma}}_{ij} + \eta_p \hat{\dot{\gamma}}_{ij} + \hat{\tau}^e_{ij}\right) \tag{7}$$

Applying the Reynolds decomposition and time-averaging the momentum balance becomes:

$$\rho U_j \frac{\partial U_i}{\partial x_j} = \frac{\partial}{\partial x_j}\left(-\overline{p} + \eta_s \dot{\Gamma}_{ij} + \eta_p \dot{\Gamma}_{ij} + T^e_{ij}\right) + \frac{\partial}{\partial x_j}\left(-\rho \overline{u_i u_j}\right), \tag{8}$$

where the Reynolds stresses will be given by the eddy viscosity model of Prandtl [21].

$$-\rho \overline{u_i u_j} = \rho C_k \sqrt{k} l \left(\frac{\partial U_i}{\partial x_j} + \frac{\partial U_j}{\partial x_i}\right) - \frac{2}{3}\rho k \delta_{ij} \tag{9a}$$

In (9a) k is the turbulent kinetic energy, which scales as u^2 (u is the scale of velocity fluctuations) and l is a large scale related both to gradients of mean flow quantities and to

the large eddies that contribute most to the turbulent kinetic energy. A parameter C_k of approximately 0.55 ensures agreement in the log-law region provided l is Prandtl's mixing length [22]. This expression is used in the context of one-equation turbulence models. Since this model will be tested in fully-developed channel flow, it is convenient to rewrite the equations in the corresponding simplified form. In this case x, y and z refer to the streamwise, wall-normal and spanwise directions with the corresponding velocity vector components being u, v and w, respectively.For a mean shear flow with mean velocity vector $U_i = (U(y), 0, 0)$, the Reynolds shear stress becomes:

$$-\rho\overline{uv} = \rho C_k \sqrt{k} l \frac{\mathrm{d}U}{\mathrm{d}y} \tag{9b}$$

and the time-averaged momentum equation reduces to:

$$-\frac{1}{\rho}\frac{\mathrm{d}\overline{p}}{\mathrm{d}x} + \left(\upsilon_s + \upsilon_p\right)\frac{d^2U}{\mathrm{d}y^2} + \frac{d}{\mathrm{d}y}\left(C_k\sqrt{k}l\frac{\mathrm{d}U}{\mathrm{d}y}\right) + \frac{1}{\rho}\frac{\mathrm{d}T^e_{xy}}{\mathrm{d}y} = 0 \tag{10}$$

In the absence of elastic effects, i.e., when the last term on the l.h.s. of (10) vanishes, average momentum balance for a Newtonian fluid with dynamic viscosity $\eta_s+\eta_p$ is recovered. Hence, the time-averaged shear stress is the direct non-Newtonian contribution to the overall momentum balance. This contribution in turn depends on the correlations between the fluctuations in elastic stress and velocity gradients, which involve all components of these two tensors. Consequently, it is important to identify the relative importance of such correlations and model the leading order terms accurately. This is discussed in the subsection below.

2.2 Time-averaged elastic stress

The time-averaged elastic stress T^e_{ij} is given by:

$$T^e_{ij} = -\eta_p\lambda\left(U_k\frac{\partial\dot{\Gamma}_{ij}}{\partial x_k} - \dot{\Gamma}_{jk}\frac{\partial U_i}{\partial x_k} - \dot{\Gamma}_{ik}\frac{\partial U_j}{\partial x_k}) - \eta_p\lambda\, C_{ij}\right. \tag{11}$$

where

$$C_{ij} = \frac{\partial^2(\overline{u_iu_k})}{\partial x_j\partial x_k} + \frac{\partial^2\left(\overline{u_ju_k}\right)}{\partial x_i\partial x_k} - 2\left(\overline{\frac{\partial u_k}{\partial x_i}\frac{\partial u_j}{\partial x_k}} + \overline{\frac{\partial u_k}{\partial x_j}\frac{\partial u_i}{\partial x_k}} + \overline{\frac{\partial u_i}{\partial x_k}\frac{\partial u_j}{\partial x_k}}\right) \tag{12}$$

Closures are required for the various terms in C_{ij}, to be discussed next. These are based on arguments of homogeneous isotropic turbulence for second order single point correlations. Evidently, near the wall, the isotropic closures are not valid. However, the objective of this analysis is to qualitatively assess the role of elastic stress-velocity gradient correlations on the mean flow. Keeping with this objective and considering the relatively simple models used for both turbulence and viscoelasticity, we employ isotropic closures. Hence, the model is more appropriate for larger Reynolds numbers for which the turbulent core is sufficiently large. According to Mathieu and Scott [23] the following relation applies to homogeneous isotropic turbulence:

$$\overline{\frac{\partial u_i}{\partial x_k}\frac{\partial u_j}{\partial x_l}} = \frac{8}{3}\frac{k}{\lambda_f^2}\left(\delta_{ij}\delta_{kl} - \frac{1}{4}\left(\delta_{ik}\delta_{jl} + \delta_{il}\delta_{jk}\right)\right) \tag{13}$$

where k is the turbulent kinetic energy and λ_f is the Taylor longitudinal microscale of turbulence.

To solve the momentum equation for fully-developed pipe or channel flows, only C_{xy} is needed (in (11) the contribution to T^e_{xy} from the terms inside the brackets is null), but it is also interesting to quantify the elastic normal stress T^e_{xx} and this requires C_{xx}. The derivation of these two C_{ij} quantities, given in (14), is presented in detail in Appendix I.

$$C_{xy} = \frac{d^2\overline{uv}}{dy^2} \text{ and } C_{xx} = -10\overline{\left(\frac{\partial u}{\partial x}\right)^2} = -\frac{40}{3}\frac{k}{\lambda_f^2} \tag{14}$$

and, from (11), the corresponding time-averaged elastic shear and polymer normal stresses are:

$$T^e_{xy} = \rho\upsilon_p\lambda\frac{d^2}{dy^2}\left(C_k\sqrt{k}l\frac{dU}{dy}\right) \tag{15}$$

$$T_{xx} = T^e_{xx} = 2\rho\upsilon_p\lambda\left(\frac{dU}{dy}\right)^2 + 10\rho\upsilon_p\lambda\overline{\left(\frac{\partial u}{\partial x}\right)^2} \tag{16}$$

To arrive at (15) the Reynolds stress model in (9b) was used. As evident from (15), the time-averaged elastic shear stress, that appears in the overall momentum balance (10), depends on the turbulent kinetic energy. As discussed below, the balance equation for k for the non-Newtonian case is influenced greatly by the polymer work, namely the correlation between the components of the fluctuating elastic stress and fluctuating velocity gradient tensors.

The C_{xx} term in (16) (second term on the right-hand-side) can be modeled invoking again turbulence isotropy, an adequate first approximation. In isotropic turbulence [23], the following relation holds for the viscous rate of dissipation (ε) taking into account its definition and (13).

$$\varepsilon = \left(\upsilon_s + \upsilon_p\right)\overline{\left(\frac{\partial u_i}{\partial x_j} + \frac{\partial u_j}{\partial x_i}\right)\frac{\partial u_j}{\partial x_i}} = 15\upsilon_T\overline{\left(\frac{\partial u_1}{\partial x_1}\right)^2} \tag{17}$$

This is based on the total kinematic viscosity of the fluid, so that back-substitution gives:

$$T_{xx} = T^e_{xx} = 2\rho\upsilon_p\lambda\left(\frac{dU}{dy}\right)^2 + \frac{2}{3}\rho\frac{\upsilon_p}{\upsilon_T}\lambda\varepsilon \tag{18}$$

We now have equations for the mean velocity and for the time-averaged normal and shear stresses as a function of k and ε for which closures must be provided.

2.3 Mean kinetic energy of turbulence and total viscous dissipation

The transport equation for the mean turbulent kinetic energy $\left(k \equiv u_i^2/2\right)$ in fully-developed shear flow is:

$$-\overline{uv}\frac{dU}{dy} + \frac{1}{\rho}\frac{d}{dy}\left(-\rho\frac{\overline{vu_i^2}}{2} - \overline{pv} + \left(\eta_s + \eta_p\right)\frac{dk}{dy} + \overline{u_i\tau^e_{iy}}\right) - \left(\upsilon_s + \upsilon_p\right)\overline{\left(\frac{\partial u_i}{\partial x_j}\right)^2} - \frac{1}{\rho}\overline{\tau^e_{ij}\frac{\partial u_i}{\partial x_j}} = 0 \tag{19}$$

where we identify the following terms:

$$\text{production of turbulence, } P_k = -\overline{uv}\frac{\mathrm{d}U}{\mathrm{d}y} \tag{20a}$$

$$\text{turbulent and molecular diffusion of } k,\ D_k = \frac{1}{\rho}\frac{d}{\mathrm{d}y}\left(-\rho\overline{\frac{vu_i^2}{2}} - \overline{pv} + \left(\eta_s + \eta_p\right)\frac{\mathrm{d}k}{\mathrm{d}y} + \overline{u_i\tau_{iy}^e}\right) \tag{20b}$$

$$\text{viscous dissipation of } k \text{ by solvent and polymer, } \varepsilon = \left(\upsilon_s + \upsilon_p\right)\overline{\left(\frac{\partial u_i}{\partial x_j}\right)^2} \tag{20c}$$

Note that the kinematic viscosity multiplied by the mean-square rate of strain is equal to the rate of viscous dissipation per unit mass defined in (17) only in homogeneous turbulence, as is assumed here. The assumption of homogeneous turbulence is typical in modeling of turbulence for shear flows [22];

$$\text{and the polymeric work, } P_w = \frac{1}{\rho}\overline{\tau_{ij}^e\frac{\partial u_i}{\partial x_j}}. \tag{20d}$$

In the diffusion of k (20b) there are four terms: the molecular diffusion, the turbulent diffusion associated with fluctuating velocities, the turbulent diffusion associated with pressure fluctuations and a new turbulent diffusion term associated with fluctuations of the elastic polymer stress. Molecular diffusion is exact and needs no modeling and the turbulent diffusion by velocity and pressure fluctuations are grouped and modeled as usual [22], invoking Boussinesq's approximation, thus introducing a turbulent Prandtl number for k (σ_k).

$$-\rho\overline{\frac{vu_i^2}{2}} - \overline{pv} = \rho\frac{C_k\sqrt{k}l}{\sigma_k}\frac{\mathrm{d}k}{\mathrm{d}y} \tag{21}$$

The turbulent diffusion due to fluctuations of the elastic polymer stress is here modeled in a similar fashion by introducing a second turbulent Prandtl number (σ_{kp}) relating turbulent kinetic energy and polymer stresses (22). Both Prandtl numbers here take the numerical value of 1.

$$\overline{u_i\tau_{iy}^e} = \rho\frac{C_k\sqrt{k}l}{\sigma_{kp}}\frac{\mathrm{d}k}{\mathrm{d}y} \tag{22}$$

A model for the total viscous dissipation is also required and here we adopt the model based on the inviscid estimate of the rate of dissipation (23), as used in Prandtl's k–l one-equation turbulence model, where l represents a turbulent length scale (here a mixing length) to be given later.

$$\varepsilon = C_D\frac{k^{3/2}}{l} \tag{23}$$

C_D=0.164 to ensure the correct log-law once an equilibrium between ε and the production of turbulent kinetic energy is assumed.

It is necessary to account for the proper behavior of dissipation close to the wall, ε_w, as is done in low Reynolds number turbulence closures. The need to use a low Reynolds number approach stems from the fact that there is no universal behavior in drag reducing fluids [24], therefore a universal law of the wall cannot be adopted and the calculations have to be carried out all the way from the bulk of the flow to the wall. The dissipation rate at the wall is:

$$\varepsilon_w = 2\left(\upsilon_s + \upsilon_p\right)\left(\frac{\partial\sqrt{k}}{\partial y}\right)_w^2 \tag{24}$$

and complies both with the wall and near wall behaviour of k [25].

Therefore, instead of using (23), the viscous dissipation is calculated with

$$\varepsilon = C_D\frac{k^{3/2}}{l} + 2\left(\upsilon_s + \upsilon_p\right)\left(\frac{\partial\sqrt{k}}{\partial y}\right)^2 \tag{25}$$

We should mention that dropping the ε_w term results in less accurate Newtonian flow predictions, but by no means the model is able to capture quantitatively all the features found in DNS calculations given its extreme simplicity. Nevertheless it qualitatively captures features of the dissipation rate in Newtonian fluids. In the next sub-section a model for the polymeric work is presented to complete the closure of the transport equation of k.

2.4 Closure for polymeric work

The polymeric work (P_w) is given by

$$P_w = \frac{1}{\rho}\overline{\tau_{ij}^e\frac{\partial u_i}{\partial x_j}} \tag{26}$$

and to propose an adequate closure we start by writing the following equation for the elastic stress fluctuations (determined as $L(\hat{\tau}_{ij}^e) - L(T_{ij}^e)$, where operator $L(\ )$ designates the corresponding stress equation based (5)):

$$\tau_{ij}^e = -\eta_p\lambda\left(\frac{\partial\dot{\gamma}_{ij}}{\partial t} + u_k\frac{\partial\dot{\Gamma}_{ij}}{\partial x_k} + u_k\frac{\partial\dot{\gamma}_{ij}}{\partial x_k} + U_k\frac{\partial\dot{\gamma}_{ij}}{\partial x_k}\right) + \eta_p\lambda\left(b_{ij} + b_{ji}\right) + \eta_p\lambda\, C_{ij} \tag{27}$$

with b_{ij} given by:

$$b_{ij} = \dot{\gamma}_{ik}\frac{\partial U_j}{\partial x_k} + \dot{\gamma}_{ik}\frac{\partial u_j}{\partial x_k} + \dot{\Gamma}_{ik}\frac{\partial u_j}{\partial x_k}. \tag{28}$$

The polymeric work is now given by (29) resulting from the product of τ_{ij}^e by $\partial u_i/\partial x_j$ and time-averaging:

$$\overline{\tau_{ij}^e\frac{\partial u_i}{\partial x_j}} = \nu_p\left[-\lambda\left(\overline{\frac{\partial\dot{\gamma}_{ij}}{\partial t}\frac{\partial u_i}{\partial x_j}} + \overline{u_k\frac{\partial u_i}{\partial x_j}\frac{\partial\dot{\Gamma}_{ik}}{\partial x_k}} + \overline{u_k\frac{\partial\dot{\gamma}_{ij}}{\partial x_k}\frac{\partial u_i}{\partial x_j}} + U_k\overline{\frac{\partial\dot{\gamma}_{ij}}{\partial x_k}\frac{\partial u_i}{\partial x_j}}\right) + \lambda\left(\overline{b_{ij}\frac{\partial u_i}{\partial x_j}} + \overline{b_{ji}\frac{\partial u_i}{\partial x_j}}\right)\right]. \tag{29}$$

Next, an order of magnitude analysis of this equation is carried out using the following scales: u is the scale of the velocity fluctuations, l is the length scale already presented above (l is related to gradients of mean flow quantities and large eddies) and λ_f is Taylor's longitudinal microscale, the length scale associated with streamwise gradients of fluctuating

streamwise quantities (in this order of magnitude analysis any Taylor microscale can be used). Hence, in the order of magnitude analysis the mean velocity will be substituted by U, any gradient of a mean flow quantity gives rise to a division by l, fluctuations of velocity inside a time average are represented by u and the length scale associated with gradients of fluctuating quantities will be substituted by Taylor's microscale. A Reynolds number is defined on the basis of the fluctuating velocity and the large eddy scale, i.e., $Re_l = \frac{ul}{\upsilon_T}$, where υ_T is the total kinematic viscosity ($\upsilon_T = \upsilon_S + \upsilon_P$). This turbulence Reynolds number is typically larger than 1 and the above two length scales are also related through it as:

$$\frac{l}{\lambda_f} \sim \sqrt{Re_l}. \tag{30}$$

We also consider steady turbulent flow, therefore the first term on the right-hand-side of (29) is:

$$\overline{\frac{\partial \dot{\gamma}_{ij}}{\partial t}\frac{\partial u_i}{\partial x_j}} = 0. \tag{31}$$

The remaining terms of (29) are of four types based on the scaling analysis. Examples of each type are shown below:

$$\begin{aligned} &1)\quad U_k\overline{\frac{\partial \dot{\gamma}_{ij}}{\partial x_k}\frac{\partial u_i}{\partial x_j}} = U_k\overline{\frac{\partial}{\partial x_k}\left(\frac{\partial u_j}{\partial x_i}+\frac{\partial u_i}{\partial x_j}\right)\frac{\partial u_i}{\partial x_j}} \propto U\frac{u^2}{\lambda_f^3},\ \text{i.e. it scales as } \frac{Uu^2}{\lambda_f^3};\\ &2)\quad \overline{\dot{\gamma}_{ik}\frac{\partial u_i}{\partial x_j}\frac{\partial U_j}{\partial x_k}} = \overline{\left(\frac{\partial u_k}{\partial x_i}+\frac{\partial u_i}{\partial x_k}\right)\frac{\partial u_i}{\partial x_j}\frac{\partial U_j}{\partial x_k}} \propto \frac{u^2}{\lambda_f^2}\frac{U}{l} \end{aligned} \tag{32a}$$

$$\text{and } \dot{\Gamma}_{ik}\overline{\frac{\partial u_j}{\partial x_k}\frac{\partial u_i}{\partial x_j}} = \left(\frac{\partial U_k}{\partial x_i}+\frac{\partial U_i}{\partial x_k}\right)\overline{\frac{\partial u_j}{\partial x_k}\frac{\partial u_i}{\partial x_j}} \propto \frac{U}{l}\frac{u^2}{\lambda_f^2}.\ \text{Using (30), one concludes that these two term scales as } \frac{Uu^2}{\lambda_f^3}\frac{1}{\sqrt{\mathrm{Re}_l}}; \tag{32b}$$

$$\begin{aligned} 3)\quad \frac{\partial \dot{\Gamma}_{ij}}{\partial x_k}\overline{u_k\frac{\partial u_i}{\partial x_j}} &= \frac{\partial}{\partial x_k}\left(\frac{\partial U_j}{\partial x_i}+\frac{\partial U_i}{\partial x_j}\right)\overline{u_k\frac{\partial u_i}{\partial x_j}}\\ &\propto \frac{Uu^2}{l^2\lambda_f}.\ \text{Using again (30), this term scale as } \frac{Uu^2}{\lambda_f^3}\frac{1}{\mathrm{Re}_l}; \end{aligned} \tag{32c}$$

$$\begin{aligned} 4)\quad \overline{u_k\frac{\partial \dot{\gamma}_{ij}}{\partial x_k}\frac{\partial u_i}{\partial x_j}} &= \overline{u_k\frac{\partial}{\partial x_k}\left(\frac{\partial u_j}{\partial x_i}+\frac{\partial u_i}{\partial x_j}\right)\frac{\partial u_i}{\partial x_j}} \propto \frac{u^3}{\lambda_f^3}\\ &\text{and } \overline{\frac{\partial u_i}{\partial x_j}\frac{\partial u_j}{\partial x_k}\frac{\partial u_i}{\partial x_k}} \propto \frac{u^3}{\lambda_f^3},\ \text{i.e. both scale as } \frac{u^3}{\lambda_f^3}. \end{aligned} \tag{32d}$$

Although the advective term 1 seems to be the largest contribution, this is actually not true because it vanishes in fully-developed steady flow. Hence, the largest contributions are actually those from the two type 4 terms, both having the same order of magnitude u^3/λ_f^3, and the remaining terms are dropped because they are divided by a large number (the Reynolds number). Note that $\overline{\frac{\partial u_i}{\partial x_j}\frac{\partial u_j}{\partial x_k}\frac{\partial u_i}{\partial x_k}}$ comes from $\overline{\dot{\gamma}_{ik}\frac{\partial u_j}{\partial x_k}\frac{\partial u_i}{\partial x_j}}$ and $\overline{\dot{\gamma}_{jk}\frac{\partial u_i}{\partial x_k}\frac{\partial u_i}{\partial x_j}}$ as part of $\overline{b_{ij}\frac{\partial u_i}{\partial x_j}}$ and $\overline{b_{ji}\frac{\partial u_i}{\partial x_j}}$ in (29), respectively, i.e., it belongs to the last term in brackets on the r.h.s. of (29). The term $\overline{u_k\frac{\partial \dot{\gamma}_{ij}}{\partial x_k}\frac{\partial u_i}{\partial x_j}}$ is the third on the r.h.s. of (29). So, this means that terms of type 4 are actually three terms in (29): one has a negative sign and two have positive signs.

In conclusion, the polymeric work of (29) can now be written as:

$$P_w = \frac{1}{\rho}\overline{\tau_{ij}^e\frac{\partial u_i}{\partial x_j}} \approx \frac{1}{\rho}\upsilon_p\left[-\lambda\,\overline{u_k\frac{\partial \dot{\gamma}_{ij}}{\partial x_k}\frac{\partial u_i}{\partial x_j}} + \lambda\left(\overline{b_{ij}\frac{\partial u_i}{\partial x_j}} + \overline{b_{ji}\frac{\partial u_i}{\partial x_j}}\right)\right] \approx A\upsilon_p\lambda\frac{u^3}{\lambda_f^3} \tag{33}$$

At first sight, parameter A can take either a positive or a negative sign, but as will be seen, with the closure developed for P_w, only a positive value of A makes sense. We shall see also that P_w can be viewed as a viscoelastic correction to the production of turbulent kinetic energy (P_k) and that this plays a role in the issue of the sign of A.

The turbulent kinetic energy transport (19) can be written in compact form as:

$$P_k - P_w + D_k - \varepsilon = 0. \tag{34}$$

From the adopted model for the Reynolds stresses (9b), the production of k is given by:

$$P_k = -\overline{u_1u_2}\frac{\mathrm{d}U}{\mathrm{d}y} = C_k\sqrt{k}l\left(\frac{\mathrm{d}U}{\mathrm{d}y}\right)^2 \tag{35}$$

To develop a closure for P_w, we start by assuming that there is equilibrium between P_k–P_w and ε, as results from inspection of (34) and the fact that diffusion of k is very small in the equilibrium region. So, $P_k - P_w = \varepsilon \rightarrow P_k = \varepsilon + P_w$. Using the inviscid approximation to estimate the rate of dissipation of k (i.e., $\varepsilon \approx u^3/l$), which is consistent with the model used in (23), the ratio μ between P_k and P_w is defined as:

$$\frac{1}{\mu} \equiv \frac{P_k}{P_w} \approx \frac{P_w+\varepsilon}{P_w} \rightarrow 1 + O\left(\frac{\varepsilon}{P_w}\right) = 1 + \frac{u^3/l}{A\upsilon_p\lambda\,u^3/\lambda_f^3} = 1 + \frac{\left(\frac{ul}{\upsilon_T}\right)\left(\frac{l}{u\lambda}\right)}{A\left(\frac{\upsilon_p}{\upsilon_T}\right)\left(\frac{l}{\lambda_f}\right)^3} \tag{36}$$

where the model for P_w in (33) was used. The normalization of (36) introduces the so-called Deborah number $\left(De_l = \frac{u\lambda}{l}\right)$ and the solvent to total viscosity ratio $\left(\beta = \frac{\upsilon_s}{\upsilon_T} = \frac{\upsilon_s}{\upsilon_s+\upsilon_p}\right)$, which, together with the relation between l and λ_f (30) gives:

$$\frac{1}{\mu} = 1 + \frac{1}{A(1-\beta)De_l\sqrt{\mathrm{Re}_l}} \rightarrow \mu = \frac{A(1-\beta)De_l\sqrt{\mathrm{Re}_l}}{1+A(1-\beta)De_l\sqrt{\mathrm{Re}_l}} \tag{37}$$

With (37) the closed expression for the polymer work based on the above equilibrium hypothesis can be written as

$$P_w = \mu P_k = \frac{AC_k(1-\beta)\lambda k^{5/4}l}{A(1-\beta)\lambda k^{3/4} + \sqrt{\upsilon_T l}}\left(\frac{\mathrm{d}U}{\mathrm{d}y}\right)^2 \tag{38}$$

after using (35) for P_k and doing $De_l = u\lambda/l$, $\mathrm{Re}_l = ul/\upsilon_T$ and also k=u^2 (one could use instead $k = 3u^2/2$, but here the 3/2 factor is contained within parameter A).

New parameters of viscoelastic constitutive models introduce new nondimensional numbers and for viscoelastic fluids one such quantity is the Deborah number which can either be viewed as the ratio of characteristic fluid and flow time scales or the ratio between elastic and viscous forces $\left(De \approx \tau^{e}_{xx}/\tau_{xy} = \eta_p \lambda \dot{\gamma}^2 \Big/ \left(\eta_p \dot{\gamma}\right) = \lambda\, U_c/L_c\right)$. In the context of the SO fluid model, devoid of memory, the second interpretation is more faithful to the physics of the model and the Deborah number measures the nonlinear deviations from Newtonian behaviour. Here, the characteristic length and velocity scales, L_c and U_c, are made identical to l and u, respectively.

2.5 Non-dimensional model equations

This analysis is finalized by presenting all relevant equations in normalized form using the friction velocity (u_τ) and the channel half height (H) as scales for velocity and length, respectively. Henceforth, superscript * denotes normalization by physical coordinates $\left(y^* = y/H\right)$, whereas the superscript + denotes normalization by wall coordinates $(y^+ = y u_\tau/\upsilon_T$ and $u^+ = u/u_\tau)$. The normalization introduces the friction Reynolds number, $\mathrm{Re}_\tau = \frac{u_\tau H}{\upsilon_T}$ and the friction Deborah number, $De_\tau = \frac{u_\tau \lambda}{H}$, where H is the channel half-width and $\upsilon_T = \upsilon_N + \upsilon_P$ is the total kinematic viscosity, the sum of the solvent and polymer kinematic viscosity coefficients. The model equations are given below. x-momentum equation:

$$1 + \frac{1}{\mathrm{Re}_\tau}\frac{d^2U^+}{\mathrm{d}y^{*^2}} + \frac{d}{\mathrm{d}y^*}\left(C_k\sqrt{k^+}l^*\frac{\mathrm{d}U^+}{\mathrm{d}y^*}\right) + \frac{\mathrm{d}T^{e^+}_{xy}}{\mathrm{d}y^*} = 0 \tag{39}$$

xy-stress equation:

$$T^+_{xy} = \frac{1-\beta}{\mathrm{Re}_\tau}\frac{\mathrm{d}U^+}{\mathrm{d}y^*} + T^{e^+}_{xy} \tag{40}$$

$$T^{e^+}_{xy} = \frac{(1-\beta)De_\tau}{\mathrm{Re}_\tau}\frac{d^2}{\mathrm{d}y^{*^2}}\left(C_k\sqrt{k^+}l^*\frac{\mathrm{d}U^+}{\mathrm{d}y^*}\right) \tag{41}$$

xx-stress equation:

$$T^+_{xx} = \frac{2(1-\beta)De_\tau}{\mathrm{Re}_\tau}\left(\frac{\mathrm{d}U^+}{\mathrm{d}y^*}\right)^2 + \frac{2(1-\beta)De_\tau \mathrm{Re}_\tau}{3}\varepsilon^+ \tag{42}$$

$$\varepsilon^+ = C_D\frac{k^{+^{3/2}}}{l^*} + \frac{2}{\mathrm{Re}_\tau}\left(\frac{\mathrm{d}\sqrt{k^+}}{\mathrm{d}y^*}\right)^2 \tag{43}$$

Mean turbulent kinetic energy equation:

$$\begin{aligned} C_k\sqrt{k^+}l^*\left(\frac{\mathrm{d}U^+}{\mathrm{d}y^*}\right)^2 - \frac{AC_k(1-\beta)\sqrt{\mathrm{Re}_\tau}De_\tau k^{+^{5/4}}l^*}{A(1-\beta)\sqrt{\mathrm{Re}_\tau}De_\tau k^{+^{3/4}} + \sqrt{l^*}}\left(\frac{\mathrm{d}U^+}{\mathrm{d}y^*}\right)^2 \\ + \frac{d}{\mathrm{d}y^*}\left[\left(\frac{C_k}{\sigma_k} + \frac{C_k}{\sigma_{kp}}\right)\sqrt{k^+}l^*\frac{\mathrm{d}k^+}{\mathrm{d}y^*}\right] + \frac{1}{Re_\tau}\frac{d^2k^+}{\mathrm{d}y^{*^2}} - \varepsilon^+ = 0 \end{aligned} \tag{44}$$

Finally, an expression is required for the large scale l^*. This large scale is related to the slope of the log-law and as a first approximation the same expression used for Newtonian fluids is used, i.e.:

$$l^* = \kappa y^* \tag{45a}$$

where κ is the von Kármán constant. However, since this turbulence model must be applied straight from the wall, including the viscous sublayer and the buffer layer, there is a damping effect that reduces l^* and a modified expression is used following the arguments of Van Driest [26] (45b):

$$l^+ = \kappa y^+ \left[1 - \exp\left(-\frac{y^+}{A^+}\right)\right] \tag{45b}$$

with A^+=26. Note that the normalization implied in (45b) uses wall coordinates, i.e., $l^+ = \frac{l u_\tau}{\nu_T}$ leading to $l^+ = l^* \mathrm{Re}_\tau$.

The numerical values of the other parameters are: C_D=0.164, $C_k = \sqrt[3]{0.164} = 0.5474$ and κ=0.41, following Newtonian literature [22]. Note that $C_\mu \equiv C_D C_k$ does not appear explicitly in this model, but this set of values is consistent with the value of C_μ=0.09 usually used. The two Prandtl numbers required in the turbulent diffusion of k are assigned unit values, i.e., $\sigma_k = \sigma_{kp} = 1$.

The sign and magnitude of parameter A affects the performance of the turbulence model; a positive value of A implies an extra dissipation due to the fluid elasticity, whereas a negative value of A leads to a more complex situation. Equations (37) and (38) imply that A>0 always leads to P_w>0 and P_w<P_k, i.e., P_w will be a correction to P_k. In contrast, for A<0, whenever $A(1-\beta)De_l\sqrt{\mathrm{Re}_l} < -0.5$, the absolute value of μ exceeds 1 and $|P_w| > |P_k|$, with $|P_w| \to \infty$ when $A(1-\beta)De_l\sqrt{\mathrm{Re}_l} \to -1$. Since De_l and Re_l are local values of Deborah and Reynolds numbers, for a particular value of A there will be a small relaxation time above which no convergence is possible due to a singularity in P_w. This is non-physical, hence a negative value of A is only acceptable provided the absolute value of the term containing A never exceeds 0.5, i.e. $A(1-\beta)De_l\sqrt{\mathrm{Re}_l} > -0.5$.

Research on DNS of channel flow for FENE-P and other differential viscoelastic model fluids [7, 11] show viscoelasticity leading to a combination of extra production and dissipation in different regions of the channel: at the edge of the viscous sublayer, there is a small amount of turbulent kinetic energy production, whereas in the log-law region the elasticity is responsible for extra dissipation of k, with the latter being significantly larger than the former. By adopting A=+1 we are thus able to test a situation where P_w is everywhere positive and its contribution reduces the production of turbulence. From a physical point of view, this can be seen, instead, as an increase in the dissipation of k, but given the specific closure adopted for P_w ($P_w \propto \partial U/\partial y$ as in the case of P_k), it makes more sense to reason in terms of turbulence production. Since adopting a negative value of A is not allowed, except for very small Deborah numbers, we tested instead the performance of a slightly modified version of P_w, from where the singularity was removed, which gives P_w<0 at the edge of the viscous sublayer and P_w>0 in the buffer and inertial sub-layers, in order to emulate qualitatively some of the findings of DNS of viscoelastic fluids described above. Such model of P_w uses the following equation:

$$P_w = \mu P_k = \frac{AC_k(1-\beta)\lambda k^{5/4} l}{A_1(1-\beta)\lambda k^{3/4} + \sqrt{\nu_T l}} \left(\frac{\mathrm{d}U}{\mathrm{d}y}\right)^2 \tag{46}$$

where A only appears in the numerator and takes the form to be discussed in Section 3.2, and the parameter A appearing in the denominator of (38) has been substituted by a positive coefficient A_1.

3 Results and Discussion

This section is divided into two parts. In Section 3.1 the performance of the model is assessed with $A=1$ and a brief set of results for $A=-1$ pertaining to sub-singularity cases which limits these calculations to very small Deborah numbers. In Section 3.2 the P_w closure of (46) is used instead of that in (38) to test a situation where viscoelasticity is responsible for turbulence production very close to the wall and enhances the dissipation of turbulent kinetic energy away from the viscous and buffer sublayers. The specific values of A and A_1 are presented in Section 3.2.

The numerical simulations were carried out with a finite volume code developed by Younis [27] for boundary layer flows, but modified here for fully-developed channel and pipe flows and also to implement the second order fluid and the currently adopted k–l turbulence model. Hence, the transport equations did not contain advective terms and the diffusive terms were discretized using second order central differences. For these fully-developed flow calculations the computational domain was a slice of the channel (with length of the order of the wall-to-wall distance), which was mapped by an orthogonal mesh containing a single column of computational cells from wall to wall; an odd number of cells was used, so there was always a cell center right on the symmetry axis and no need to impose symmetry boundary conditions. Periodic boundary conditions were set to relate the transverse profiles of velocity and turbulent kinetic energy at the inlet and outlet and for the streamwise pressure gradient the procedure of Patankar and Spalding [28] was adopted. The pressure was calculated in a staggered mesh to ensure pressure-velocity coupling and the tridiagonal set of algebraic equations was solved with tridiagonal matrix algorithm (TDMA). At the walls the velocities and k were set to zero. The non-uniform mesh used had between 99 and 199 cells from wall to wall and at least 5 control volumes were located within each viscous sublayer ($y^+<5$). A mesh convergence study was carried out initially to quantify the uncertainty of the results and Richardson's extrapolation to the limit was used to estimate the correct result, a standard procedure according to Roache [29]. The use of a mesh with 199 cells from wall-to-wall provided results with accuracy below 0.1% (in which case there were about 12 cells within each of the two viscous sublayers) and the use of 99 cells from wall-to-wall gave results with an accuracy better than 1%.

3.1 Predictions for $A=+1$ and at small values of Deborah number for $A=-1$

One set of calculations was carried out to assess the effect of fluid elasticity upon fully-developed pipe flow considering that viscoelasticity is responsible for reducing turbulent kinetic energy production ($A=+1$). Results for three sub-critical flow conditions are also presented in some plots using $A=-1$, meaning very small Deborah numbers so that the singularity in the denominator of (38) never appears. The conditions corresponding to all these simulations are summarized in Table 1. The friction Reynolds number and the friction Deborah number were defined in the previous section. The table also lists the values of Deborah (De) and Reynolds (Re) numbers based on the bulk velocity in the channel.

The drag reduction (DR) was proportional to the value of Deborah number and for these parameters high values of DR (of the order of 38%) were attained for very small values of

Table 1 Variation of the Darcy friction factor and drag reduction as a function of De_τ at Re_τ=1,046

$De_\tau \times 10^3$	De	Re	β	f	DR (%)	A
0	0	20,000	1	0.0219	–	1
0	0	20,000	0.8	0.0219	–	1
2.02	0.04	20,675	0.8	0.0205	6.4	1
3.96	0.08	21,115	0.8	0.0197	10.2	1
9.54	0.2	21,950	0.8	0.0182	17.0	1
18.4	0.4	22,800	0.8	0.0169	23.0	1
35.1	0.8	23,815	0.8	0.0154	29.5	1
82.2	2.0	25,450	0.8	0.0135	38.3	1
0.21	0.004	19,920	0.8	0.0221	−0.8	−1
0.42	0.008	19,820	0.8	0.0223	−1.8	−1
1.08	0.02	19,420	0.8	0.0232	−6.1	−1

De_τ. The drag reduction is here defined as the relative difference between the calculated friction factor and the corresponding Newtonian friction factor at the same friction Reynolds number. Note that no calibration of the turbulence model against experimental data was carried out, hence the use of A=+1 is purely arbitrary and serves the purpose of a qualitative assessment. In fact, in a real situation these amounts of drag reduction take place at larger values of De_τ, an indication that a more realistic value of A would be smaller. For a Newtonian fluid $(De, De_\tau = 0)$ the turbulence model performs identically, as it should, regardless of the distribution of the total viscosity by η_p and η_s. This is shown in the first two lines of both tables pertaining to β=1 and 0.8, respectively. There are small differences between the predictions by the current turbulence model for Newtonian fluid and known data from the literature, such as the Blasius-type equation for the friction factor and the log-law. These differences are due to the limitations of the k–l turbulence model of Prandtl used here, but they are small and irrelevant in the context of the proposed objectives.

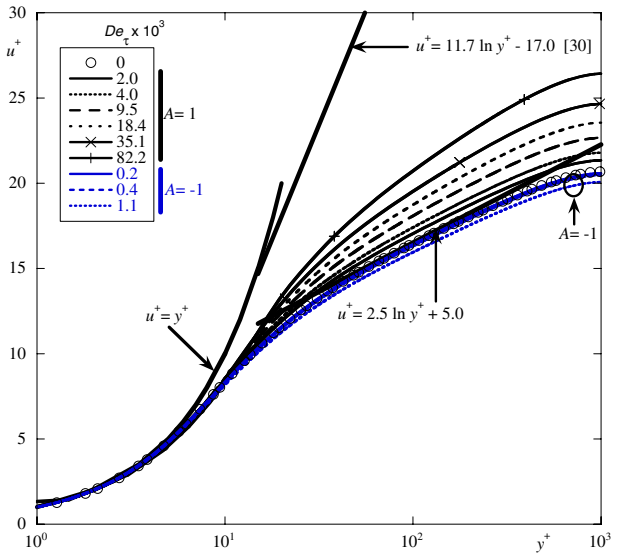

Fig. 1 Effect of friction Deborah number on the mean velocity profiles in channel flow for Re_τ= 1,046 and β=0.8 using A=1 (*black*) and A=−1 (*blue*)

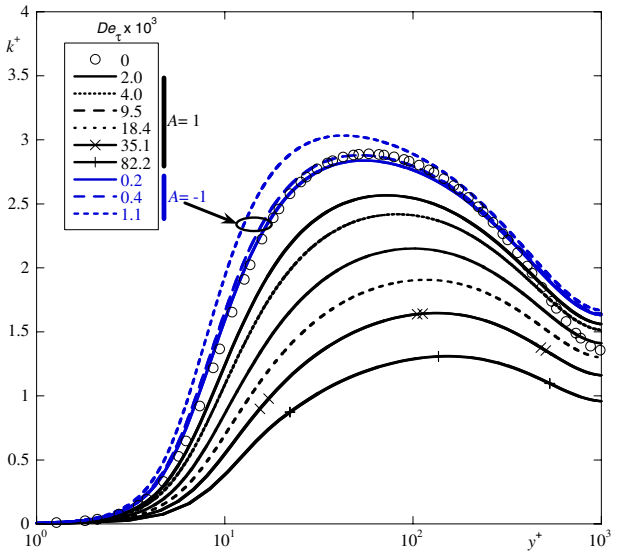

Fig. 2 Effect of friction Deborah number on the profile of normalized turbulent kinetic energy in channel flow for Re_τ=1,046 and β=0.8 using A=1 (*black*) and A=−1 (*blue*)

In Fig. 1 velocity profiles are plotted in wall coordinates and compared with the Newtonian log-law and the maximum drag reduction asymptote of Virk et al. [30] for polymer solutions. For the Newtonian fluid the profile approaches the standard log-law, except near the centerline where it tends to level off. With A=+1, there is a progressive upwards shift in the velocity as the Deborah number increases, consistent with the increasing levels of drag reduction. In contrast, for the three sub-critical simulations with negative values of A we see a drag increase and the corresponding downward shift of the log law. In all cases, near the wall the velocity profiles coincide with the viscous sublayer expression (u^+=y^+) and at high values of y^+, but away from the centerline, the slope of the

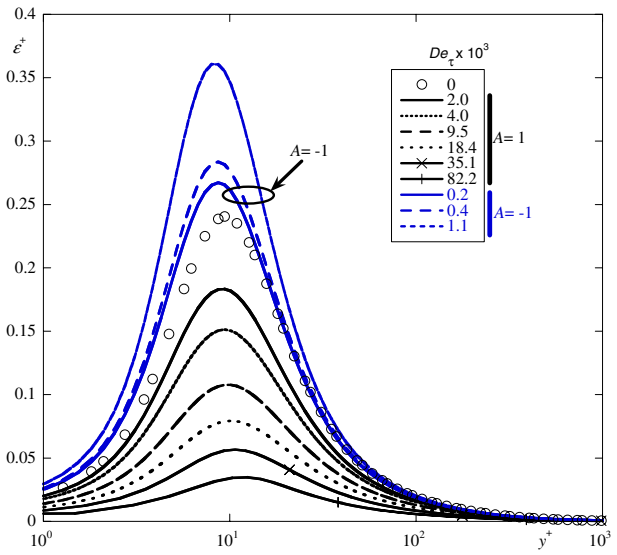

Fig. 3 Effect of friction Deborah number on the profile of the rate of dissipation of turbulent kinetic energy in channel flow at Re_τ= 1,046 and β=0.8 using A=1 (*black*) and A=−1 (*blue*)

log-law remains the same as for Newtonian fluids. This is to be expected from the imposed model for the large length scale l (45) since the slope of the velocity profile in the inertial region is inversely proportional to the value of κ which was kept unmodified. For A=+1, this behavior is typical of that found for polymer solutions at low and moderate drag reductions.

The corresponding profiles of the normalized turbulent kinetic energy $\left(k^+ = k/u_\tau^2\right)$ are plotted in Fig. 2, and here the situation is partially different from that seen with DR fluids. In the presence of drag reduction (A=+1) k^+ is continuously decreasing as De_τ increases and simultaneously its peak is moving away from the wall. This continuous decrease in the peak k^+ is in contrast with the literature for low drag reduction, where k^+ remains basically

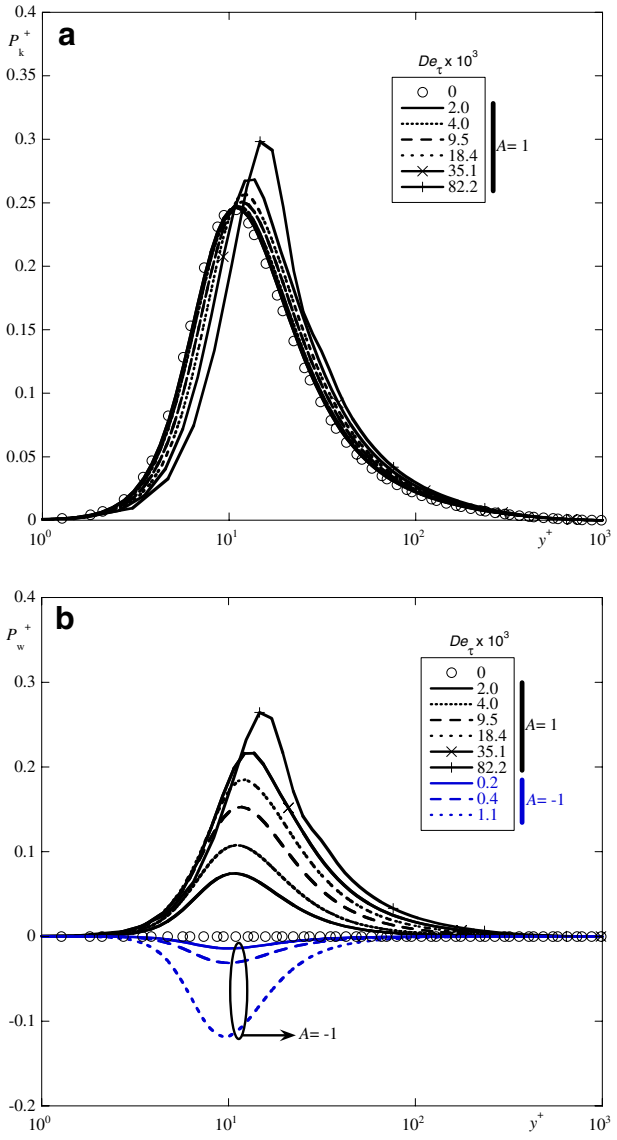

Fig. 4 Effect of friction Deborah number and A on the profiles of **a** P_k^+, **b** P_w^+, **c** $P_k^+ - P_w^+$ for channel flow at Re_τ=1,046 and β=0.8 using A=1 (*black*) and A=−1 (*blue*)

Fig. 4 (continued)

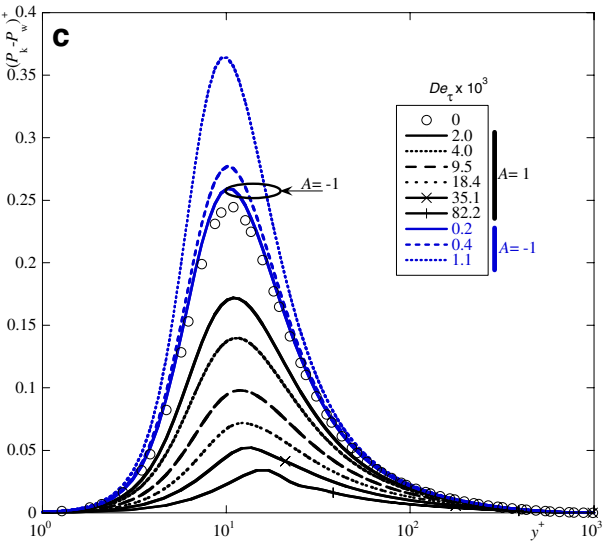

unchanged. In fact, for polymer solutions, the streamwise normal Reynolds stress increases initially with DR compensating for the decrease in the radial and transverse normal Reynolds stresses. Here, in contrast, k^+ always decreases with De_τ and since this is an isotropic turbulence model, the predicted individual normal Reynolds stresses qualitatively behave as k^+. In the turbulent core we see an increase in k^+ at low DR followed by a decrease at large DR, whereas the DNS data for viscoelastic fluids with memory in the literature shows a constant k^+ at low DR followed by a decrease at large DR. In agreement with the DNS data is the fact that the location of the peak k^+ moves away from the wall as DR increases.

For the drag increase simulations obtained with $A=-1$ the profiles of k^+ are shifted upwards everywhere and the peak moves closer to the wall. This situation is not typical of polymer solutions and also suggests that the use of a negative constant value of A is unphysical.

In Fig. 3 the effect of De_τ on the normalized rate of dissipation $\left(\varepsilon^+ = \varepsilon \upsilon_T / u_\tau^4\right)$ is shown and an intense decrease in ε^+ is observed as De_τ increases, when $A=+1$. The peak dissipation is always seen to happen at the same location, at $y^+ \approx 9$. DNS results for Newtonian [31] and polymer [7] channel flows show the maximum dissipation to occur at the wall rather than in the buffer layer, but this deficiency of the adopted simple turbulence model does not affect the objective of the present work. Since the dissipation is decreasing with De_τ and there is drag reduction accompanied by a reduction in k^+, the production of turbulence must also be decreasing as well, as is investigated in more detail in Fig. 4. For $A=-1$ the opposite trend is seen.

The three plots of Fig. 4 represent three quantities in normalized form: the production of k due to the interaction between the Reynolds stress and the mean velocity gradient (P_k) in Fig. 4a, the polymer work (P_w) in Fig. 4b and the difference between these two quantities, which essentially must balance the total rate of dissipation near the wall, is shown in Fig. 4c. These three quantities have all been normalized by the quantity used to normalize the rate of dissipation, u_τ^4/ν_T, as required from (34).

Except for the two simulations at $De_\tau \times 10^3$ of 35.1 and 82.2, the amount of drag reduction is not too large, hence the Reynolds stresses and the mean velocity profiles are

not too different and so the production of turbulence, P_k^+, does not change by much, as seen in Fig. 4a. The actual dimensional P_k decreases with the Deborah number because of the reduction in Reynolds shear stress corresponding to the calculated drag reduction, whereas the slight increase in P_k^+ is a consequence of the reduced friction velocity used in the normalization. Regarding the polymer contribution P_w^+, Fig. 4b shows that it depends on De_τ acting to reduce the production of turbulence for positive values of A ($P_w>0$) and to increase production of turbulence for negative values of A ($P_w<0$), i.e., leading to drag reduction and drag increase, respectively. As a result, the difference $P_k^+ - P_w^+$, plotted in Fig. 4c, decreases with De_τ for $A=+1$ and increases for $A=-1$ in order to equilibrate the dissipation ε^+. Since the dissipation is proportional to turbulence, according to the theory, the drag reduction for $A>0$ is a consequence of an equilibrium between $P_k^+ - P_w^+$ and ε^+

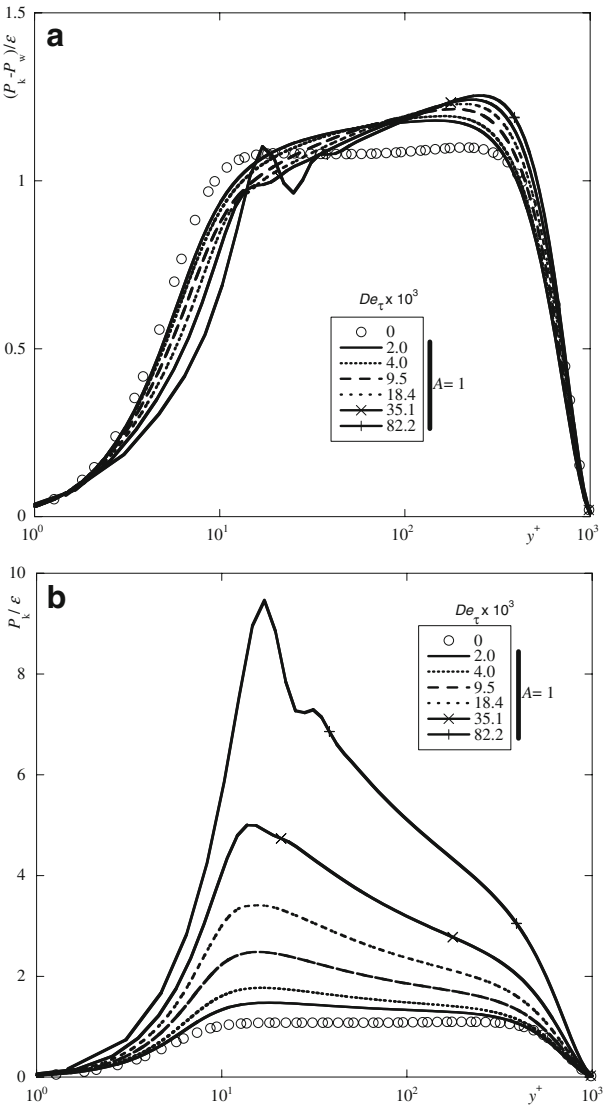

Fig. 5 Effect of friction Deborah number on the profile of $\frac{P_k - P_w}{\varepsilon_N}$ (**a**) and $\frac{P_k}{\varepsilon_N}$ (**b**) for channel flow at Re_τ=1,046 and β=0.8 using A=+1

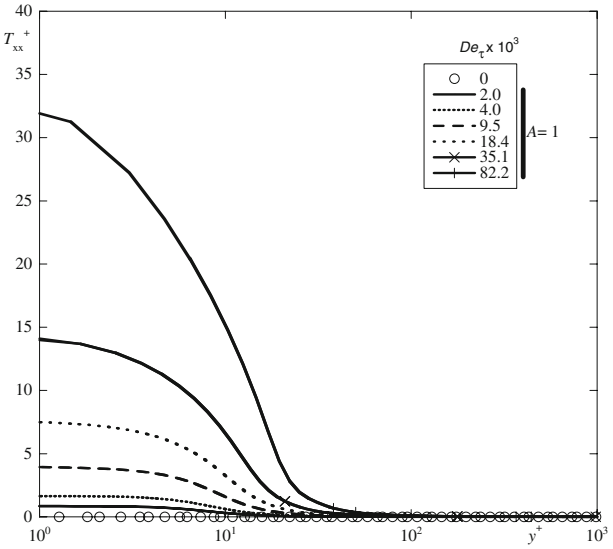

Fig. 6 Effect of friction Deborah number on the normalized profile of the elastic normal stress for channel flow at Re_τ=1,046 and β=0.8 using A=+1

reached for lower levels of turbulence and hence of lower Reynolds stresses. This equilibrium is shown in Fig. 5a to be quite similar to that observed for Newtonian fluids. The DNS results for memory fluids do not exhibit such an intense increase in P_w, but the mechanism of drag reduction is also more complex than a second order fluid could provide due to interactions absent here, such as strain-hardening.

At large Deborah numbers, there are strong variations in the elastic shear stress very close to the wall (see (15)) creating some convergence problems and oscillations. This is also clear in the oscillation seen in the profile at $De_\tau \times 10^3 = 82.2$ in Fig. 5b which is the outcome of a difference of two large values. Figures 4 and 5 also confirm that $P_w < P_k$, but they tend to be equal as the Deborah number increases, and hence the drag reduction,

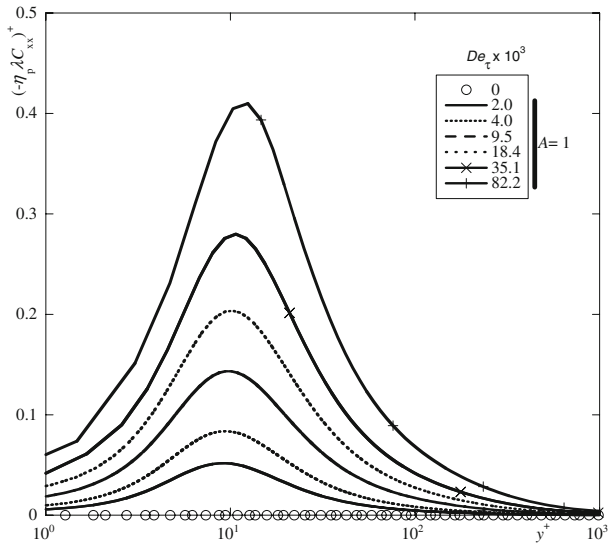

Fig. 7 Effect of friction Deborah number on the normalized profile of the turbulent contribution to the elastic normal stress for channel flow at Re_τ=1,046 and β=0.8 using A=+1

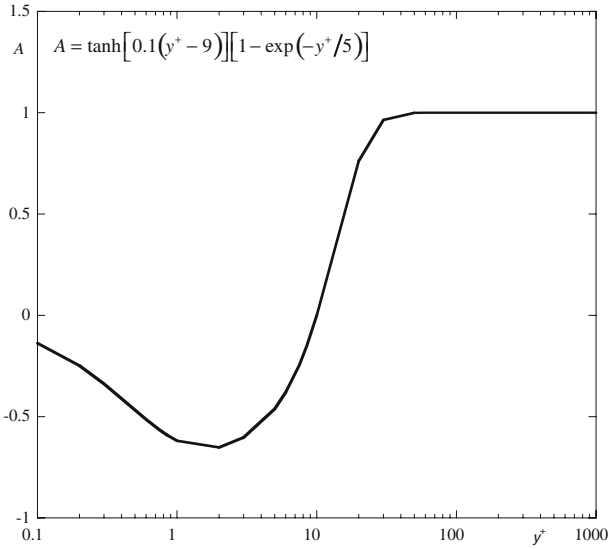

Fig. 8 Imposed variation of parameter A with distance to the wall in wall coordinates

is increased. Given the unphysical nature of the model with $A=-1$ no further results for this case will be shown.

The effect of elasticity upon the time-averaged elastic normal stress is shown in Figs. 6 and 7. In Fig. 6 the total stress T_{xx}^+ is plotted, whereas Fig. 7 only shows the contribution from turbulence (second term on the right-hand-side of (16)). The mean flow contribution to the elastic normal stress dominates by two orders of magnitude, as is seen from a direct comparison between the two figures. An interesting difference between the two contributions to the elastic normal stress, obvious from inspection of (16), is that the molecular contribution peaks at the wall, since it is proportional to the mean velocity gradient, whereas the turbulent contribution peaks where ε is maximum.

3.2 Alternative model for P_w

Here we assess the performance of an alternative model for P_w, that of (46), with $A_1=1$ and a variable form for A, in order to create a region of negative P_w very close to the wall (viscoelasticity enhancing production of turbulent kinetic energy close to the wall) and a region of positive P_w in the inertial sub-region (viscoelasticity reducing turbulent kinetic

Table 2 Variation of the Darcy friction factor and drag reduction as a function of De_τ at $Re_\tau=1{,}046$ for variable A

$De_\tau \times 10^3$	De	Re	β	f	DR (%)
0	0	20,000	0.8	0.0219	–
2.04	0.04	20,417	0.8	0.0210	4.0
4.05	0.08	20,694	0.8	0.0205	6.5
9.86	0.2	21,225	0.8	0.0194	11.2
19.2	0.4	21,759	0.8	0.0185	15.5
37.2	0.8	22,515	0.8	0.0173	21.1

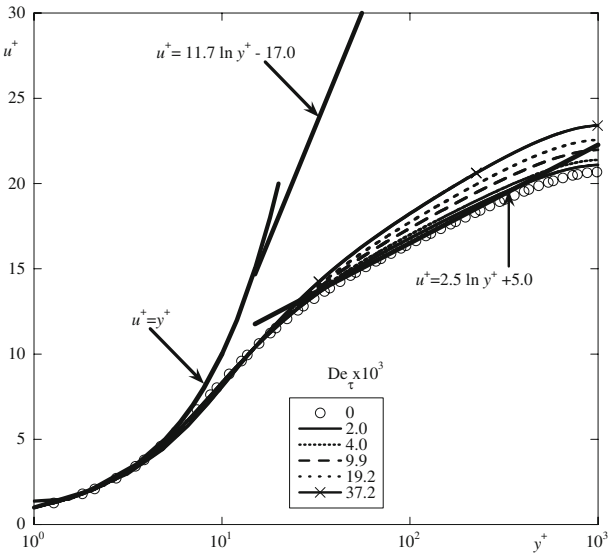

Fig. 9 Effect of friction Deborah number on the mean velocity profiles in channel flow for Re_τ= 1,046 and β=0.8 using a variable A according to (47)

energy production), in an attempt to emulate what has been found in the DNS calculations with differential viscoelastic constitutive equations. For that purpose, parameter A takes the form of (47) plotted in Fig. 8. The numerical value of y^+_{crit} is arbitrary, but similar to the value where the viscoelastic stress work for FENE-P fluids changes from negative to positive in [7] and more specifically in the data of Li et al. (2006; Personal communication and DNS data set for FENE-P channel flow) for $\text{Re}_\tau = 395$, $De_\tau = 25$, L=30, β=0.9 and a drag reduction of 18%. The function used to quantify parameter A was formulated taking into account the following conditions from inspection of data in Li et al. (2006; Personal communication and DNS data set for FENE-P channel flow): it accounts for low Reynolds

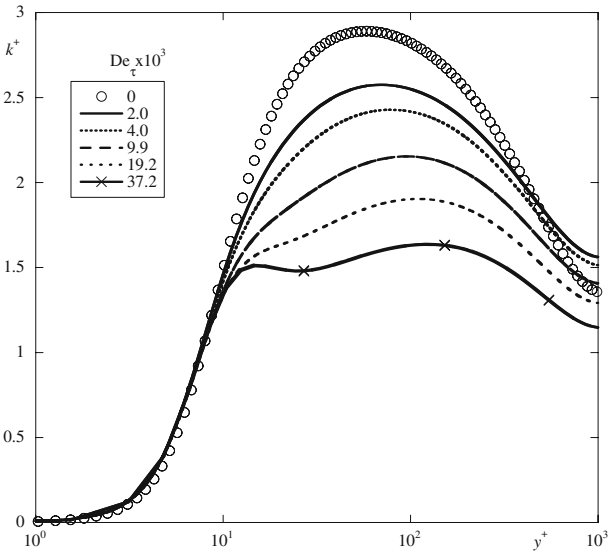

Fig. 10 Effect of friction Deborah number on the profile of normalized turbulent kinetic energy in channel flow for Re_τ=1,046 and β=0.8 using a variable A according to (47)

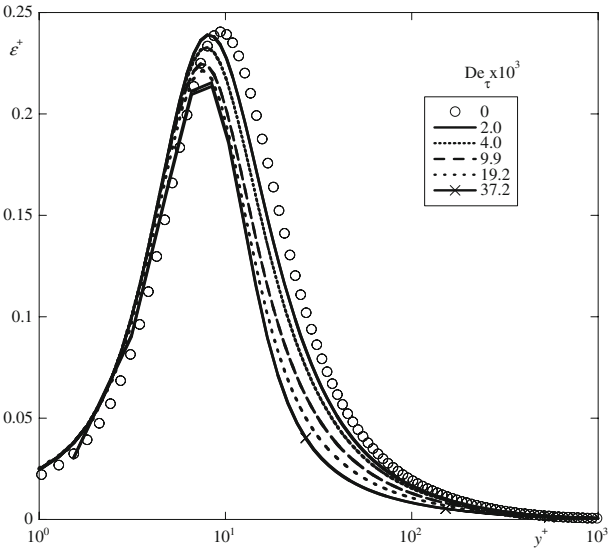

Fig. 11 Effect of friction Deborah number on the profile of the rate of dissipation of turbulent kinetic energy in channel flow at Re_τ=1,046 and β=0.8 using a variable A according to (47)

number effects and it should have no effect for $y^+ \geq 50$; A=0 for y=0; there should be a negative peak in P_w at the edge of the viscous sublayer and its sign should change to positive at $y^+ \approx 9$ to 10. A possible function obeying these conditions is:

$$A = \tanh\left[0.1\left(y^+ - y^+_{\text{crit}}\right)\right]\left[1 - \exp(-y^+/5)\right] \text{ with } y^+_{\text{crit}} = 9 \tag{47}$$

The simulations carried out with this model are listed in Table 2 and the plots of Figs. 9, 10, 11, 12, 13 discuss these results in more detail. In all cases drag reduction is obtained, even though there is now a small region close to the wall where P_w produces turbulent kinetic energy, as explained above. Elsewhere, P_w remains dissipative as for A=+1.

Now, the drag reduction is less than for the corresponding Deborah numbers with A=+1 and this is also the outcome of lower absolute values of A for $y^+ < 50$ (c.f. Fig. 8). The mean velocity profiles in Fig. 9 show the corresponding upwards shift and the turbulent kinetic energy profiles of Fig. 10 exhibit the reduction already seen in Fig. 2, i.e. there is nothing fundamentally different in these two last plots from a qualitative point of view.

In contrast, the plot of ε^+ in Fig. 11 shows important qualitative differences relative to Fig. 3. The decrease in ε^+ with DR is smaller than in Fig. 3 and in the viscous and buffer sub-layers there is actually an increase in ε^+ compatible with the role of P^+_w, since in this region P^+_w acts as an extra production of turbulence, as shown in Fig. 12b and so the dissipation must rise to compensate. The variations of P_k and P_w inside the channel are plotted in Fig. 12: the profiles of P^+_k are essentially unchanged, apart from a small increase in the inertial sub-layer, but of lesser magnitude than in Fig. 4. P^+_w, shown in Fig. 12b, has the desired trend with the adoption of the variable parameter A in (47): negative in the viscous and buffer layers and positive elsewhere, with the Deborah number raising $\left|P^+_w\right|$ everywhere. The consequent total production of turbulent kinetic energy, $P^+_k - P^+_w$, close to the wall and its peak value at $y^+ \approx 10$ remains essentially constant, a result totally unexpected and different from the strong decrease seen in Fig. 4c, whereas in the inertial sub-layer a reduction in $P^+_k - P^+_w$ is seen as previously for A=+1.

The plot of Fig. 13a shows that now there is less local equilibrium than with A=+1, even though that equilibrium seems to continue to exist on average in the inertial sub-layer; the ratio $(P_k - P_w)/\varepsilon$ is not constant at 1.1 as for De=0, but oscillates around the Newtonian plateau. It takes values above the Newtonian plateau at the edges of the inertial layer and below the plateau well inside the log-law region. The variation of P_k/ε with De_τ is not as strong as seen for A=+1, but is qualitatively similar. These oscillations in $(P_k - P_w)/\varepsilon$ result from the breakdown of the equilibrium condition $((P_k - P_w) \approx \varepsilon)$ at $y^+ \leq 10$ (c.f. Fig. 8), which was imposed to develop the closure of P_w in Section 2.4.

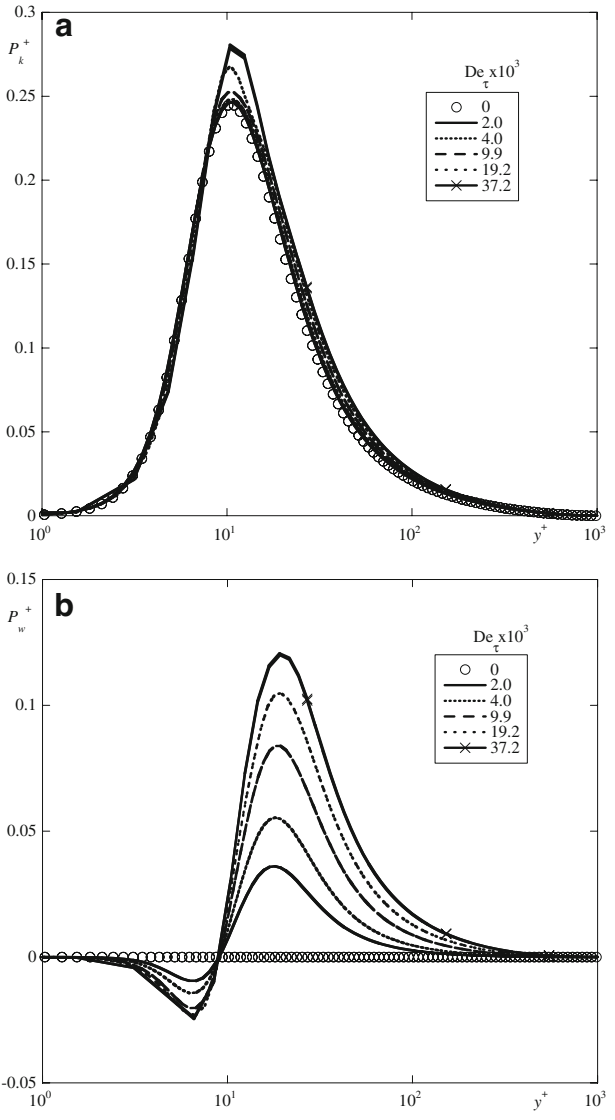

Fig. 12 Effect of friction Deborah number and A on the profiles of **a** P_k^+, **b** P_w^+, **c** $P_k^+ - P_w^+$ for channel flow at Re_τ=1,046 and β=0.8 using a variable A according to (47)

Fig. 12 (continued)

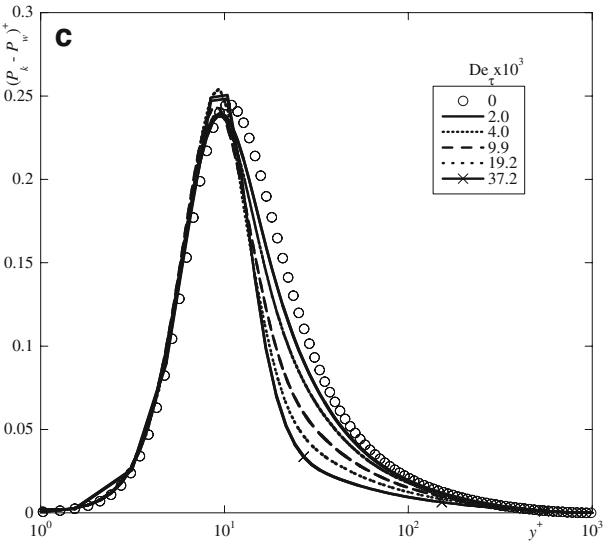

4 Conclusions

A simplified version of the second order viscoelastic constitutive equation is used to derive a simple turbulence closure of the *k–l* type to investigate qualitatively the effects of elastic normal and shear stresses upon fully-developed channel flow of viscoelastic fluids. Specifically, the second order correction to the Newtonian constitutive equation results into one extra term in the balance of momentum proportional to the gradient of the time-average elastic shear stress and two extra terms in the balance of *k*. The time average elastic shear stress in turn depends on gradients of *k* and was found to have a small impact. The two extra contributions in the balance of *k* are a small viscoelastic turbulent transport term of negligible impact and an important interaction between all the components of the fluctuating elastic stress and rate of strain tensors, here denoted by P_w, for which a closure is developed to evaluate its effect on predicting turbulent drag reduction. The development of this closure is based on arguments of homogeneous isotropic turbulence and of equilibrium in boundary layer flows and introduces a parameter. Despite the simplicity of the constitutive model and approximations involved, the results clearly demonstrate that the sign of this extra term must be positive ($P_w>0$), i.e., P_w should act to reduce the production of turbulent kinetic energy, to predict DR. In this case the model predictions qualitatively agree with DNS data for viscoelastic fluids, with exceptions to this agreement being associated with deficiencies in the *k–l* base turbulence model rather than on the closure developed for P_w. In contrast, using a negative value for the parameter appearing in the model of P_w leads to drag increase at very low Deborah number flows, and numerical breakdown of the model to a model singularity. An alternative closure for P_w, mimicking the viscoelastic stress work in DNS of FENE-P fluids, was also tested successfully. This alternative model resulted also in drag reduction, in spite of the enhancement of turbulence production very close to the wall, but the equilibrium conditions in the inertial sublayer were not so strongly maintained.

In conclusion, even in the simplified descriptions of fluid elasticity and turbulence used in this work, the interaction between fluctuating polymer stresses and fluctuating rates of

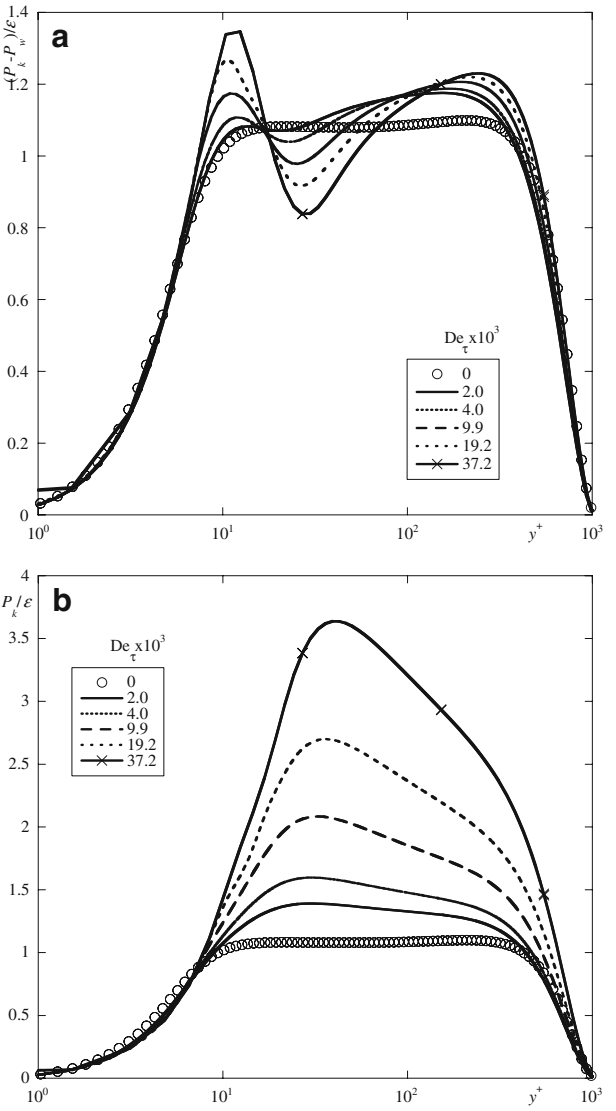

Fig. 13 Effect of friction Deborah number on the profile of $\frac{P_k - P_w}{\varepsilon_N}$ (**a**) and $\frac{P_k}{\varepsilon_N}$ (**b**) for channel flow at Re_τ=1,046 and β=0.8 using a variable A according to (47)

strain has a direct bearing on the predicted drag reduction. These interactions can be modeled by mimicking DNS data, which shows that they dissipate turbulent kinetic energy in the channel except for a small region of turbulence production close to the wall. This leads to the prediction of DR. If instead, an enhancement of turbulence production takes place in the inertial sublayer, as a consequence of fluid elasticity, then a drag increase in observed.

Acknowledgements FT Pinho acknowledges the funding from Fundação Calouste Gulbenkian (Scholarship 72259) and Fundação para a Ciência e a Tecnologia (Scholarship SFRH/BSAB/507/2005). Funding from FEDER and FCT via project POCI/56342/EQU/2004 is also gratefully acknowledged. Partial support from the NSF funding through grant CTS 9874813 (R.S.) is acknowledged.

Appendix I

For fully-developed pipe or channel flows only the shear component of the extra term C_{ij} of the time-average elastic stress, defined in (12), is required. Since the fluid is elastic, there is also a non-zero normal stress of elastic origin, which requires C_{xx}. To obtain these two components, we start with (12), here rewritten as (48):

$$C_{ij} = \frac{\partial^2 \overline{(u_i u_k)}}{\partial x_j \partial x_k} + \frac{\partial^2 \overline{(u_j u_k)}}{\partial x_i \partial x_k} - 2\left(\overline{\frac{\partial u_k}{\partial x_i}\frac{\partial u_j}{\partial x_k}} + \overline{\frac{\partial u_k}{\partial x_j}\frac{\partial u_i}{\partial x_k}} + \overline{\frac{\partial u_i}{\partial x_k}\frac{\partial u_j}{\partial x_k}}\right) \tag{48}$$

and use the relation between fluctuating strain rates for homogeneous isotropic turbulence [23]. These equations are written in the indicial notation introduced by Einstein:

$$\overline{\frac{\partial u_i}{\partial x_k}\frac{\partial u_j}{\partial x_l}} = \frac{8}{3}\frac{k}{\lambda_f^2}\left(\delta_{ij}\delta_{kl} - \frac{1}{4}\left(\delta_{ik}\delta_{jl} + \delta_{il}\delta_{jk}\right)\right) \tag{49}$$

For C_{xy}, i=1 and j=2, hence (48) becomes:

$$C_{xy} = C_{12} = \frac{\partial^2 \overline{(u_1 u_k)}}{\partial x_2 \partial x_k} + \frac{\partial^2 \overline{(u_2 u_k)}}{\partial x_1 \partial x_k} - 2\left(\overline{\frac{\partial u_k}{\partial x_1}\frac{\partial u_2}{\partial x_k}} + \overline{\frac{\partial u_k}{\partial x_2}\frac{\partial u_1}{\partial x_k}} + \overline{\frac{\partial u_1}{\partial x_k}\frac{\partial u_2}{\partial x_k}}\right) \tag{50}$$

For fully-developed flow only $\partial/\partial y \neq 0$. Therefore, the first two terms on the right-hand-side (rhs) of (50) become:

$$\begin{aligned}\frac{\partial^2 \overline{(u_1 u_k)}}{\partial x_2 \partial x_k} + \frac{\partial^2 \overline{(u_2 u_k)}}{\partial x_1 \partial x_k} &= \frac{\partial^2 \overline{(u_1 u_1)}}{\partial x_2 \partial x_1} + \frac{\partial^2 \overline{(u_1 u_2)}}{\partial x_2 \partial x_2} + \frac{\partial^2 \overline{(u_1 u_3)}}{\partial x_2 \partial x_3} + \frac{\partial^2 \overline{(u_2 u_1)}}{\partial x_1 \partial x_1} \\ &+ \frac{\partial^2 \overline{(u_2 u_2)}}{\partial x_1 \partial x_2} + \frac{\partial^2 \overline{(u_2 u_3)}}{\partial x_1 \partial x_3} = \frac{\partial^2 \overline{(u_1 u_2)}}{\partial x_2 \partial x_2} = \frac{d^2 \overline{(uv)}}{dy}\end{aligned} \tag{51}$$

The first term inside the brackets of (50) expands to become:

$$\overline{\frac{\partial u_k}{\partial x_1}\frac{\partial u_2}{\partial x_k}} = \overline{\frac{\partial u_1}{\partial x_1}\frac{\partial u_2}{\partial x_1}} + \overline{\frac{\partial u_2}{\partial x_1}\frac{\partial u_2}{\partial x_2}} + \overline{\frac{\partial u_3}{\partial x_1}\frac{\partial u_2}{\partial x_3}}. \tag{52}$$

Each of these three terms is substituted by (49) and after application of the rule δ_{ij}=0 when $i \neq j$ and δ_{ij}=1 when $i=j$, the following result appears naturally:

$$\overline{\frac{\partial u_1}{\partial x_1}\frac{\partial u_2}{\partial x_1}} = \frac{8}{3}\frac{k}{\lambda_f^2}\left(\delta_{12}\delta_{11} - \frac{1}{4}(\delta_{11}\delta_{21} + \delta_{11}\delta_{21})\right) = 0 \tag{53a}$$

$$\overline{\frac{\partial u_2}{\partial x_1}\frac{\partial u_2}{\partial x_2}} = \frac{8}{3}\frac{k}{\lambda_f^2}\left(\delta_{22}\delta_{12} - \frac{1}{4}(\delta_{21}\delta_{22} + \delta_{22}\delta_{21})\right) = 0, \text{ and} \tag{53b}$$

$$\overline{\frac{\partial u_3}{\partial x_1}\frac{\partial u_2}{\partial x_3}} = \frac{8}{3}\frac{k}{\lambda_f^2}\left(\delta_{32}\delta_{13} - \frac{1}{4}(\delta_{31}\delta_{23} + \delta_{33}\delta_{21})\right) = 0 \tag{53c}$$

Similarly, for the second term inside the brackets of (50),

$$\overline{\frac{\partial u_k}{\partial x_2}\frac{\partial u_1}{\partial x_k}} = \overline{\frac{\partial u_1}{\partial x_2}\frac{\partial u_1}{\partial x_1}} + \overline{\frac{\partial u_2}{\partial x_2}\frac{\partial u_1}{\partial x_2}} + \overline{\frac{\partial u_3}{\partial x_2}\frac{\partial u_1}{\partial x_3}} \tag{54}$$

where

$$\overline{\frac{\partial u_1}{\partial x_2}\frac{\partial u_1}{\partial x_1}} = \frac{8}{3}\frac{k}{\lambda_f^2}\left(\delta_{11}\delta_{2l} - \frac{1}{4}(\delta_{12}\delta_{11} + \delta_{11}\delta_{12})\right) = 0 \tag{55a}$$

$$\overline{\frac{\partial u_2}{\partial x_2}\frac{\partial u_1}{\partial x_2}} = \frac{8}{3}\frac{k}{\lambda_f^2}\left(\delta_{21}\delta_{22} - \frac{1}{4}(\delta_{22}\delta_{12} + \delta_{22}\delta_{12})\right) = 0, \text{ and} \tag{55b}$$

$$\overline{\frac{\partial u_3}{\partial x_2}\frac{\partial u_1}{\partial x_3}} = \frac{8}{3}\frac{k}{\lambda_f^2}\left(\delta_{31}\delta_{23} - \frac{1}{4}(\delta_{32}\delta_{13} + \delta_{33}\delta_{12})\right) = 0 \tag{55c}$$

For the third term, the corresponding expressions are:

$$\overline{\frac{\partial u_1}{\partial x_k}\frac{\partial u_2}{\partial x_k}} = \overline{\frac{\partial u_1}{\partial x_1}\frac{\partial u_2}{\partial x_1}} + \overline{\frac{\partial u_1}{\partial x_2}\frac{\partial u_2}{\partial x_2}} + \overline{\frac{\partial u_1}{\partial x_3}\frac{\partial u_2}{\partial x_3}} \tag{56}$$

$$\overline{\frac{\partial u_1}{\partial x_1}\frac{\partial u_2}{\partial x_1}} = \frac{8}{3}\frac{k}{\lambda_f^2}\left(\delta_{12}\delta_{11} - \frac{1}{4}(\delta_{11}\delta_{21} + \delta_{11}\delta_{21})\right) = 0 \tag{57a}$$

$$\overline{\frac{\partial u_1}{\partial x_2}\frac{\partial u_2}{\partial x_2}} = \frac{8}{3}\frac{k}{\lambda_f^2}\left(\delta_{12}\delta_{22} - \frac{1}{4}(\delta_{12}\delta_{22} + \delta_{12}\delta_{22})\right) = 0, \text{ and} \tag{57b}$$

$$\overline{\frac{\partial u_1}{\partial x_3}\frac{\partial u_2}{\partial x_3}} = \frac{8}{3}\frac{k}{\lambda_f^2}\left(\delta_{12}\delta_{33} - \frac{1}{4}(\delta_{13}\delta_{23} + \delta_{13}\delta_{23})\right) = 0 \tag{57c}$$

In conclusion, $C_{xy} = \frac{d^2\overline{(uv)}}{dy}$.

A similar procedure is now applied for C_{xx} without further comments. Starting from (48):

$$C_{xx} = C_{11} = 2\frac{\partial^2\overline{(u_1u_k)}}{\partial x_1\partial x_k} - 2\left(2\overline{\frac{\partial u_k}{\partial x_1}\frac{\partial u_1}{\partial x_k}} + \overline{\frac{\partial u_1}{\partial x_k}\frac{\partial u_1}{\partial x_k}}\right) \tag{58}$$

The first term on the rhs of (58) is:

$$\frac{\partial^2\overline{(u_1u_k)}}{\partial x_1\partial x_k} = \frac{\partial^2\overline{(u_1u_1)}}{\partial x_1\partial x_1} + \frac{\partial^2\overline{(u_1u_2)}}{\partial x_1\partial x_2} + \frac{\partial^2\overline{(u_1u_3)}}{\partial x_1\partial x_3} = 0. \tag{59}$$

The first term inside the brackets of (58) is:

$$\overline{\frac{\partial u_k}{\partial x_1}\frac{\partial u_1}{\partial x_k}} = \overline{\frac{\partial u_1}{\partial x_1}\frac{\partial u_1}{\partial x_1}} + \overline{\frac{\partial u_2}{\partial x_1}\frac{\partial u_1}{\partial x_2}} + \overline{\frac{\partial u_3}{\partial x_1}\frac{\partial u_1}{\partial x_3}} \tag{60}$$

The correlations above can be evaluated as follows:

$$\overline{\frac{\partial u_1}{\partial x_1}\frac{\partial u_1}{\partial x_1}} = \frac{8}{3}\frac{k}{\lambda_f^2}\left(\delta_{11}\delta_{11} - \frac{1}{4}(\delta_{11}\delta_{11} + \delta_{11}\delta_{11})\right) = \frac{4}{3}\frac{k}{\lambda_f^2} \tag{61a}$$

$$\overline{\frac{\partial u_2}{\partial x_1}\frac{\partial u_1}{\partial x_2}} = \frac{8}{3}\frac{k}{\lambda_f^2}\left(\delta_{21}\delta_{12} - \frac{1}{4}(\delta_{21}\delta_{12} + \delta_{22}\delta_{11})\right) = -\frac{2}{3}\frac{k}{\lambda_f^2}, \text{ and} \tag{61b}$$

$$\overline{\frac{\partial u_3}{\partial x_1}\frac{\partial u_1}{\partial x_3}} = \frac{8}{3}\frac{k}{\lambda_f^2}\left(\delta_{31}\delta_{13} - \frac{1}{4}(\delta_{31}\delta_{13} + \delta_{33}\delta_{11})\right) = -\frac{2}{3}\frac{k}{\lambda_f^2} \tag{61c}$$

These three terms add to zero.
The second term inside the brackets is:

$$\overline{\frac{\partial u_1}{\partial x_k}\frac{\partial u_1}{\partial x_k}} = \overline{\frac{\partial u_1}{\partial x_1}\frac{\partial u_1}{\partial x_1}} + \overline{\frac{\partial u_1}{\partial x_2}\frac{\partial u_1}{\partial x_2}} + \overline{\frac{\partial u_1}{\partial x_3}\frac{\partial u_1}{\partial x_3}} \tag{62}$$

$$\overline{\frac{\partial u_1}{\partial x_1}\frac{\partial u_1}{\partial x_1}} = \frac{8}{3}\frac{k}{\lambda_f^2}\left(\delta_{11}\delta_{11} - \frac{1}{4}(\delta_{11}\delta_{11} + \delta_{11}\delta_{11})\right) = \frac{4}{3}\frac{k}{\lambda_f^2} \tag{63a}$$

$$\overline{\frac{\partial u_1}{\partial x_2}\frac{\partial u_1}{\partial x_2}} = \frac{8}{3}\frac{k}{\lambda_f^2}\left(\delta_{11}\delta_{22} - \frac{1}{4}(\delta_{12}\delta_{12} + \delta_{12}\delta_{12})\right) = \frac{8}{3}\frac{k}{\lambda_f^2}, \text{ and} \tag{63b}$$

$$\overline{\frac{\partial u_1}{\partial x_3}\frac{\partial u_1}{\partial x_3}} = \frac{8}{3}\frac{k}{\lambda_f^2}\left(\delta_{11}\delta_{33} - \frac{1}{4}(\delta_{13}\delta_{13} + \delta_{13}\delta_{13})\right) = \frac{8}{3}\frac{k}{\lambda_f^2} \tag{63c}$$

These three terms above add to $\frac{20}{3}\frac{k}{\lambda_f^2}$. Backsubstituting in (58) gives the following result:

$$C_{xx} = -\frac{40}{3}\frac{k}{\lambda_f^2} = -10\overline{\frac{\partial u}{\partial x}\frac{\partial u}{\partial x}} \tag{64}$$

References

1. Warholic, M.D., Heist, D.K., Katcher, M., Hanratty, T.J.: A study with particle-image velocimetry of the influence of drag-reducing polymers on the structure of turbulence. Exp. Fluids **31**, 474–483 (2001)
2. Warholic, M.D., Massah, H., Hanratty, T.J.: Influence of drag reducing polymers on turbulence: effects of Reynolds number, concentration and mixing. Exp. Fluids **27**, 461–472 (1999)

3. Ptasinski, P.K.M., Nieuwstadt, F.T., Brule, B.H.A.A.V.D., Hulsen, M.A.: Experiments in turbulent pipe flow with polymer additives at maximum drag reduction. Flow Turbul. Combust **66**, 159–182 (2001)
4. Escudier, M.P., Presti, F., Smith, S.: Drag reduction in the turbulent pipe flow of polymers. J. Non-Newton. Fluid Mech **81**, 197–213 (1999)
5. Ptasinski, P.K., Boersma, B.J., Nieuwstadt, F.T.M., Hulsen, M.A., den Brule, B.H.A.A.V., Hunt, J.C.R.: Turbulent channel flow near maximum drag reduction: simulations, experiments and mechanisms. J. Fluid Mech **490**, 251–291 (2003)
6. Dimitropoulos, C.D., Sureshkumar, R., Beris, A.N.: Direct numerical simulation of viscoelastic turbulent channel flow exhibiting drag reduction: effect of the variation of rheological parameters. J. Non-Newton. Fluid Mech **79**, 433–468 (1998)
7. Dimitropoulos, C.D., Sureshkumar, R., Beris, A.N., Handler, R.A.: Budgets of Reynolds stress, kinetic energy and streamwise enstrophy in viscoelastic turbulent channel flow. Phys. Fluids **13**, 1016–1027 (2001)
8. Dimitropoulos, C.D., Dubief, Y., Shaqfeh, E.S.G., Moin, P., Lele, S.K.: Direct numerical simulation of polymer-induced drag reduction in turbulent boundary layer flow. Phys. Fluids **17**, 11705 (2005)
9. Housiadas, K.D., Beris, A.N.: An efficient fully implicit spectral scheme for DNS of turbulent viscoelastic channel flow. J. Non-Newton. Fluid Mech **122**, 243–262 (2004)
10. Angelis, E.D., Casciola, C.M., Piva, R.: DNS of wall turbulence: dilute polymers and self-sustaining mechanisms. Comput. Fluids **31**, 495–507 (2002)
11. Kim, K., Li, C.-F., Sureshkumar, R., Balachandar, S., Adrian, R.: Effects of polymer stresses on eddy structures in drag-reduced turbulent channel flow. J. Fluid Mech **584**, 281–299 (2007)
12. Li, C.-F., Gupta, V.K., Sureshkumar, R., Khomami, B.: Turbulent channel flow of dilute polymeric solutions: drag reduction scaling and an eddy viscosity model. J. Non-Newton. Fluid Mech **139**, 177–189 (2006)
13. Shaqfeh, E.S., Iaccarini, G., Shi, M.: A RANS model for turbulent drag reduction by polymer injection and comparison to DNS. Paper FM2, The Society of Rheology 78th Annual Meeting, October 8–12, 2006, Portland, Maine, USA (2006)
14. Cruz, D.O.A., Pinho, F.T., Resende, P.R.: Modeling the new stress for improved drag reduction predictions of viscoelastic pipe flow. J. Non-Newton. Fluid Mech **121**, 127–141 (2004)
15. Resende, P.R., Escudier, M.P., Presti, F., Pinho, F.T., Cruz, D.O.A.: Numerical predictions and measurements of Reynolds normal stresses in turbulent pipe flow of polymers. Int. J. Heat Fluid Flow **27**, 204–219 (2006)
16. Resende, P.R., Pinho, F.T., Cruz, D.O.A.: Performance of the *k–e* and Reynolds stress models in turbulent flows with viscoelastic fluids. Proceedings of the 11th Brazilian Congress of Thermal Sciences and Engineering–ENCIT 2006, Curitiba, Brazil, Dec 5–8 2006, paper CIT06-0805.pdf (2006)
17. Elata, C., Poreh, M.: Momentum transfer in turbulent shear flow of an elastico-viscous fluid. Rheol. Acta **5**, (2), 148–151 (1966)
18. Roy, A., Morozov, A., van Saarloos, W., Larson, R.G.: Mechanism of polymer drag reduction using a low-dimensional model. Phys. Rev. Lett **97**, 234501 (2006)
19. Tanner, R.I.: Engineering Rheology. Clarendon, Oxford (1985)
20. Bird, R.B., Armstrong, R.C., Hassager, O.: Dynamics of Polymeric Liquids. Volume 1: Fluid Mechanics. Wiley, New York (1987)
21. Prandtl, L.: Über ein neues Formelsystem für die ausgebildete Turbulenz, pp. 6–19. Mathematik–Physik Klasse, Nachrichten Akademisches Wissenschaft, Göttingen (1945)
22. Pope, S.B.: Turbulent Flows. Cambridge University Press, Cambridge, UK (2000)
23. Mathieu, J., Scott, J.: An Introduction to Turbulent Flow, pp. 267–268. Cambridge University Press, Cambridge, UK (2000)
24. Hoyt, J.W.: The effect of additives on fluid friction. J. Basic Eng **94**, 258–285 (1972)
25. Patel, V.C., Rodi, W., Scheuerer, G.: Turbulence models for near-wall and low Reynolds number flows: a review. AIAA J **23**, 1308–1319 (1984)
26. Van Driest, R.E.: On turbulent flow near a wall. J. Aeronaut. Sci **23**, 1007–1011 (1956)
27. Younis, B.A.: A computer program for two-dimensional turbulent boundary layer flows. Internal report, Department of Civil Engineering, City University, London, UK (1987)
28. Patankar, S.V., Spalding, D.B.: A calculation procedure for heat, mass and momentum transfer in three-dimensional parabolic flows. Int. J. Heat Mass Transfer **15**, 1787–1806 (1972)
29. Roache, P.J.: Quantification of uncertainty in computational fluid mechanics. Annu. Rev. Fluid Mech **29**, 123–160 (1997)
30. Virk, P.S., Mickley, H.S., Smith, K.A.: The ultimate asymptote and mean flow structure in Toms Phenomena. J. Appl. Mech **92**, 488–493 (1970)
31. Mansour, N.N., Kim, J., Moin, P.: Reynolds stress and dissipation rate budgets in a turbulent channel flow. J. Fluid Mech **194**, 15–44 (1988)